Modelling Cancer Dynamics Using Cellular Automata

Álvaro G. López, Jesús M. Seoane, and Miguel A. F. Sanjuán

Abstract Cellular automata and agent-based models have become the cornerstone of the simulation of many complex biological phenomena. More specifically, they are making major breakthroughs in the understanding of cancer development. Besides, these discrete spatio-temporal models can be hybridized with more traditional models based on differential equations, allowing to faithfully represent multiscale open systems. These systems typically consist of many entities that can perform a vast repertoire of actions, which depend on the concentration of substances diffused in their environments, as well as their mutual interaction through different coupling mechanisms. In the present chapter, we use a hybrid cellular automaton model to explore the dynamics of tumor growth in the presence of an immunological response. A mathematical expression is derived, which describes the speed at which a tumor is erased by a population of immune cytotoxic cells, depending on the morphology of the tumors and the intrinsic capacity of the immune cells to detect and destroy their adversaries. Finally, the coevolution of tumor–immune aggregates is simulated and the likelihood of a prolonged tumor mass dormancy mediated by the immune system is discussed.

Keywords Cancer dynamics · Cellular automata · Tumour growth · Immune cells · Mathematical modelling

Á. G. López · J. M. Seoane
Nonlinear Dynamics, Chaos and Complex Systems Group, Departamento de Física, Universidad Rey Juan Carlos, Móstoles, Madrid, Spain
e-mail: alvaro.lopez@urjc.es

M. A. F. Sanjuán (✉)
Nonlinear Dynamics, Chaos and Complex Systems Group, Departamento de Física, Universidad Rey Juan Carlos, Móstoles, Madrid, Spain

Department of Applied Informatics, Kaunas University of Technology, Kaunas, Lithuania

Institute for Physical Science and Technology, University of Maryland, College Park, MD, USA
e-mail: miguel.sanjuan@urjc.es

F. Berezovskaya, B. Toni (eds.), *Advanced Mathematical Methods in Biosciences and Applications*, STEAM-H: Science, Technology, Engineering, Agriculture, Mathematics & Health,
https://doi.org/10.1007/978-3-030-15715-9_8

PACS 05.45.Ac, 05.45.Df, 05.45.Pq

1 Introduction

The oversimplification of cancer as the growth of an independent subset of rebel mutated cells within a tissue presents great difficulties explaining tumor development [1, 2]. The relative importance of the dynamics at the tissue level during carcinogenesis, represented by the interactions of the tumor cells with their environment, compared to the role played by mutations, or in connection with them, is still a subject of intense debate [3, 4]. Perhaps, in order to unveil the origin of cancer, a fundamental question that needs to be addressed first is why healthy somatic cells, as part of a tissue, do not grow unlimitedly. It is hard to believe that eukaryotic cells have lost their ability to reproduce in the absence of growth factors, since autopoiesis pervades life at all scales. Assuming this fact, we would then have to understand how a tissue as a whole self-organizes contributing to this suppression and control of cell growth. Undoubtedly, chemical and physical interactions between both similar and different types of cells within the tissue should play a key role in differentiation and tumorigenesis. The tumor microenvironment includes stromal cells (e.g., immune cells, fibroblasts, or endothelial cells), the extracellular matrix, and signalling molecules such as cytokines or growth factors. The particular cellular and molecular mechanisms, as well as their role in tumor development, are complex and not sufficiently well understood [5]. Even though all of them might prove to be important in the fight against cancer, immunotherapy is lately focusing great attention. Probably, this is because the immune system is better known and has evolved for centuries to neatly destroy threatening foreign organisms in our body. As it occurs with any other evolutionary entity, when a tumor forms, it should develop its own biochemical imprints (antigens), which would allow for its recognition by the immune system. Therefore, there is evidence and hope that it can be trained to effectively destroy tumor cells, which originate in the body, as well.

The history of immunotherapy for cancer dates back to the beginning of the twentieth century, when the physician Paul Ehrlich suggested that the immune system might protect an organism from the development of cancer [6]. Around 50 years later, this proposition was more formally reintroduced by Macfarlane Burnet [7, 8] and, later on, by Lewis Thomas [9]. After suffering major setbacks [10, 11], the immunosurveillance theory gained renewed consistence close to 20 years ago, thanks to several experimental works with genetically altered mice [12, 13]. Currently, the immunosurveillance of tumors is more properly referred as cancer immunoediting. Given the genetic heterogeneity of tumors, this control system coevolves with them and seems to act as a natural selective force, editing its phenotype by selecting those cells that are unresponsive to immune detection.

Adoptive cell transfer using chimeric antigen receptors [14, 15], the modulation of CTLA-4 activity by means of monoclonal antibodies [16], or the blocking of the PD-1 receptor [17] are a few outstanding examples of the increasing importance that

immunotherapy is gaining. Nevertheless, and despite some dramatic cases of cure, the advantages of immunotherapy are still modest in general, and only some cancers (less than 10%) might benefit from immunotherapy nowadays [18]. Therefore, there is still a long way to go in the investigation of immunotherapy for cancer, as the many ongoing clinical trials indicate [19]. The progress of tumor immunotherapy with T lymphocytes mainly relies on our capacity to uncover and understand the molecular and cellular basis of the T-cell-mediated antitumor response. However, due to the highly complex regulatory mechanisms that control both cell growth and the immune system, this task can be hardly achieved without the use of mathematical models. From a theoretical point of view, these models provide an analytical framework in which fundamental questions concerning cancer dynamics can be addressed in a rigorous fashion. The practical reason for their development is to make quantitative predictions that permit the refinement of the existing therapies or even the design of new ones.

Because cancer is a biological phenomenon occurring at multiple scales, mathematical models of tumor growth are becoming increasingly sophisticated. In particular, agent-based modelling and cellular automata are the groundbreaking instruments of contemporary research in the study of cancer dynamics [20–25]. These models allow to accurately represent the cell heterogeneity within a tissue, and can be hybridized with more traditional models based on differential equations, which allow to represent the substances that diffuse through the tissue and the intracellular dynamics as well. More particularly, mathematical models describing a growing tumor that interacts with the cellular arm of the immune system have demonstrated their potential to explain different properties of tumor–immune interactions [26].

In the present work, we adopt the view of enzyme kinetics to describe tumor–immune interactions at the cellular scale [27, 28]. Enzymatic reactions can be viewed in an abstract manner as an asymmetric interaction between two entities, one being rather passive (the substrate) and the other being rather active (the enzyme). When these two entities make contact, the latter affects the former transforming it into some other entity (the product). Thus, an enzymatic reaction can be casted in three steps: the formation of a complex from the two parts, a subsequent transformation of the passive part by its active counterpart and their final dissociation. As long as these conditions are fulfilled, there is no general reason preventing us to use this conceptual framework not only at the chemical scale, but also at the cellular scale and, perhaps, even at higher scales. For example, the growth of microorganisms in the presence of a limited substrate obeys the Michaelis–Menten kinetics [29]. In ecology, the intake rate of a consumer as a function of the density of preys is also a kinetics of this type [30]. In all these cases, whenever there is a considerable imbalance between the number of active and passive elements, saturation occurs. This is due to the limited capacity of the active part to interact with a sufficiently high number of elements of the passive counterpart. Note that, in part, this is also true in the reverse direction, since the passive elements cannot interact with an enormous number of active elements for short times. Nevertheless, the situation is not completely symmetrical, since an active element can interact

with many passive elements, while a passive element usually interacts with one or a few active elements, before it is transformed. In summary, interactions occur locally and require some time.

Inspired by this reasoning, a mathematical model describing tumor–immune interactions was designed by Kuznetsov et al. [31] to explore a possible dynamical origin of the dormancy and the sneaking through of tumors. In their original model, the rate at which a tumor is lysed increases linearly with the number of immune cells, just as in an ordinary Lotka–Volterra model [32, 33]. Simply put, the velocity at which a tumor is destroyed can be increased without bounds by simply adding more immune cells. Nevertheless, their work served as a foundation for other works concerning the interactions between immune and tumor cells [34, 35]. Among these works, a mathematical model was validated using experiments from mice [36] and men [37]. To reproduce the experimental data, these authors proposed a new fractional cell kill for the lysis of tumor cells by $CD8^+$ lymphocytes. The fractional cell kill is a key concept in the study of tumor lysis, which has sometimes been confused with the rate of tumor cell lysis, because the notion of rate is used in a loose sense [35, 38]. However, strictly speaking, these concepts are different. The rate represents the speed at which the tumor is lysed, while the fractional cell kill is defined as the speed at which the logarithm of the tumor size is reduced. Well, these authors noticed that the lysis curves seen in experimental settings exhibited saturation. Briefly, the fraction of lysed tumor cells after a certain time (usually a few hours in chromium release assays) versus different values of the initial effector-to-target ratio saturates for increasing values of the latter. Therefore, they proposed a Hill function [38, 39] depending on the effector-to-target ratio as the mathematical function describing the rate at which a tumor is lysed. Their brilliant achievement notwithstanding, little theoretical explanation was given to this function and the original proposal [31] was partly forgotten.

In this chapter, we use several cellular automata models to characterize more rigorously the nature of the mathematical expression that governs the lysis of tumor cells by cytotoxic cells. Our study indicates that this mathematical function emerges from spatial and geometrical restraints. Interestingly, simulations are provided in the limit of immunodeficient environments, where saturation becomes less evident. We demonstrate that the current mathematical function works bad for such environments, and retake the conceptual framework of enzyme kinetics to propose another fractional cell kill. We show that this new function behaves better in the limit in which the immune cell population is small compared to the tumor size, and that the parameters appearing in it have a clear physical and biological interpretation. Then, we investigate the kinetics of tumor lysis in different limiting situations. This second analysis allows us to further explore the mathematical expression. As we will see, to reproduce also the time series as well as the lysis curves, one last rearrangement must be introduced, which we believe makes it theoretically more conspicuous. To conclude, we explore the transient and asymptotic dynamics that results from the coevolution of a growing tumor and the cell-mediated immune response. A cellular automaton is used to analyze the correspondence between this dynamics and the three phases of the theory of immunoedition: elimination,

equilibrium, and escape. The exploration of different immunological scenarios enables the discussion of a possible dynamical origin of tumor dormancy and the sneaking through of tumors, as originally proposed by Kuznetsov et al. [31]. Our results demonstrate that the immune system can keep a tumor dormant for long periods of time, but that this dormancy is based on a frail equilibrium between the mechanisms that spur the immune response and the growth of the tumor. Thus, we question the capacity of the cell-mediated immune response to sustain long periods of dormancy, as those appearing in recurrent disease. We suggest that its role might be rather to synergize with other types of tumor dormancy.

2 Model Description

2.1 A Hybrid Cellular Automaton Model

The simulations are accomplished by means of a cellular automaton (CA) model developed in [40] to study the interactions between tumor and immune effector cells. This model was built on a previously CA model designed to study the effects of competition for nutrients and growth factors in avascular tumors [41]. It is hybrid because the cells are treated discretely, allowing them to occupy several grid points in a particular spatial domain, and evolve according to probabilistic and direct rules. On the other hand, the diffusion of nutrients (such as glucose and oxygen) or growth factors from the vessels into such spatial region is represented through linear reaction–diffusion equations, which are continuous and deterministic. We expose separately the equations governing the diffusion of substances and the rules describing the behavior of cells.

2.1.1 Diffusion of Nutrients

Two types of nutrients are utilized in this model, making a distinction between those which are specific for cell division $N(x, y, t)$, and others $M(x, y, t)$ that are related to the remaining cellular activities. The partial differential equations for the diffusion of nutrients are

$$\frac{\partial N}{\partial t} = D_N \nabla^2 N - k_1 T N - k_2 H N - k_3 E N \tag{1}$$

$$\frac{\partial M}{\partial t} = D_M \nabla^2 M - k_4 T M - k_5 H M - k_6 E M, \tag{2}$$

where $T(x, y, t)$, $H(x, y, t)$, and $E(x, y, t)$ are functions representing the number of tumor, healthy, and immune cells at time t and position (x, y). For simplicity, we assume that both types of nutrients have the same diffusion coefficient $D_N = D_M = D$. Following [40], we consider that the competition parameters are equal $k_2 = k_3 =$

$k_5 = k_6 = k$, except for the tumor cells, which compete more aggressively. We set $k_1 = \lambda_N k$ and $k_4 = \lambda_M k$, with λ_M and λ_N greater than one. An adiabatic limit is considered, assuming that the solutions are stationary. This approximation holds because the time it takes a tumor cell to complete its cell cycle, which is of the order of days [42], is much longer than that of the diffusion of nutrients. A quadrilateral domain $\Omega = [0, L] \times [0, L]$ is considered and Dirichlet boundary conditions are imposed on the vertical sides of the domain, where the vessels are placed, assigning $N(0, y) = N(L, y) = N_0$ and $= M(0, y) = M(L, y) = M_0$. For simplicity, the horizontal upper and lower bounds of the domain obey periodic boundary conditions $N(x, 0) = N(x, L)$ and $M(x, 0) = M(x, L)$, wrapping them together to form a cylinder. Finally, the diffusion equations are nondimensionalized as explained in [41], and the equations are numerically solved by using finite-difference methods with successive overrelaxation. The resolution of the grid n equals 300 pixels in all our simulations. We describe these two steps before enumerating the CA rules.

2.1.2 Cellular Automata Rules

Since the CA used in the last part of the present work is just a variation of the one used in the first analysis, here we simply present the CA rules and the algorithm for this first study. The modifications latter required are introduced along the way. The study of the lysis of tumors with different morphologies is carried out in two successive steps. The first is devoted to the growth of the tumors, while the second focuses on their lysis by the CTLs.

1. We generate distinct solid tumors as monoclonal growths, arising after many iterations of the cellular automaton. At each CA iteration the tumor cells can divide, move, or die attending to certain probabilistic rules that depend on the nutrient concentration per tumor cell and some specific parameters. Each of these parameters θ_a represent the intrinsic capacity of the tumor cells to carry out a particular action a. The precise probabilistic laws and the corresponding actions are described ahead in detail. Attending to morphology, diverse types of tumors can be generated, depending on the nutrient competition parameters among tumor cells α, λ_N. We simulate four types of geometries (spherical, papillary, filamentary, and disconnected), and inspect four tumors of different sizes for each shape.
2. The lysis of tumor cells is a hand-to-hand struggle comprising several processes. After recognition of these cells through antigen presentation via MHC class I molecules, the $CD8^+$ T cells proceed to induce apoptosis. The principal mechanism involves the injection of proteases through pores on the cell membrane that have been previously opened by polymerization of perforins. Even though death may take about an hour to become evident, it takes minutes for a T cell to program antigen-specific target cells to die [43]. We assign a time of 10 min for each iteration of the CA, and other choices can be made. Therefore, twenty-four iterations of the CA equal the 4 h after which the lysis of tumor cells is measured

in the experiments [36]. Since the cell cycle time of a tumor cell is generally a few times longer, we assume a second adiabatic approximation and suspend the tumor cell dynamics during T cell lysis.

The rules governing the effector cells evolution are as follows. At each iteration, those immune cells that are in contact with at least one tumor cell might lyse them with certain probability. The intrinsic cytotoxic capability, which in the model also accounts for the capacity of T cells to recognize tumor cells [44], is related to the parameter θ_{lys}. If a T cell destroys a tumor cell, recruitment might be induced in its neighboring CA elements. When immune cells are not in direct contact with a tumor cell, they can either move or become inactivated. Thus, the present CA model does not represent T cell infiltration into the tumor mass, which is discussed somewhere else [45]. We consider that a single T cell cannot lyse more than three times, leaving the region of interest when this occurs [40]. The precise probabilistic laws and the corresponding actions are again thoroughly described ahead. Each of the sixteen solid tumors is co-cultivated with different effector-to-target ratios as initial conditions (see Fig. 1) and the lysis is computed 4 h later.

Because our study mainly focuses on how fast lymphocytes lyse a tumor, an important simplification between our cellular automaton and the one presented in [40] deserves notification. We have excluded a constant source of NK cells from

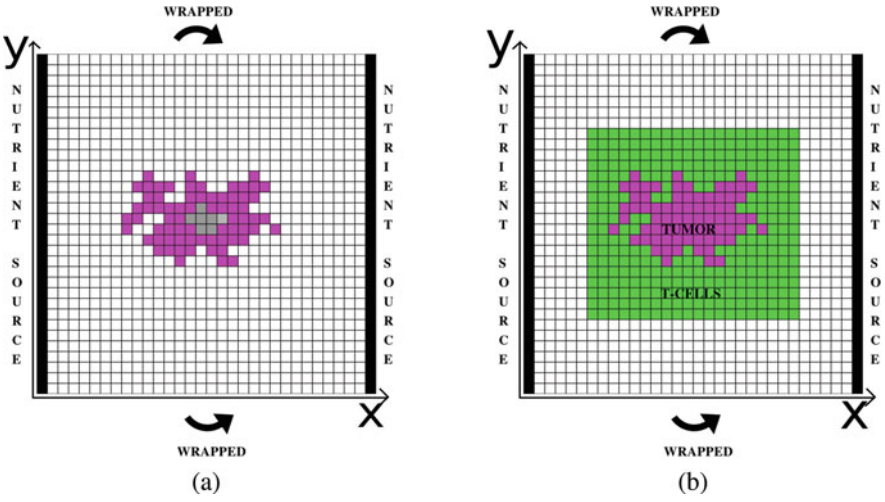

Fig. 1 (**a**) Schematic representation of the cellular automaton grid in a square domain, with some tumor cells (pink) growing from its center, and some necrotic cells (gray) at its core. Two vertical vessels on the boundary supply the nutrients required for cell division and other cellular activities. The upper and lower bounds are identified, forming a cylinder. (**b**) To study the lysis of the tumors, the initial conditions are always prepared by randomly placing the effector cells in a rectangular region outside the tumor. The size of this domain is selected so that for the maximum values of the effector-to-target ratio the region is almost filled with effector cells

the model. The CA rules are now described for the two steps, one corresponding to the development of the tumors, and the other related to the lysis of the tumor cells by the cytotoxic T cells. They are almost the same as those used in [40], and any difference will be explicitly remarked. In what follows, $T(\vec{x})$ and $E(\vec{x})$ are the tumor and immune cells at position $\vec{x}$, while $N(\vec{x})$ and $M(\vec{x})$ are the concentration of nutrients in nondimensional variables at position $\vec{x}$. $N(\vec{x})$ represents those nutrients required for cell division, and $M(\vec{x})$ those required for other cellular activities. The role of the healthy cells is simplified to passive competitors for nutrients that allow the tumor cells to freely divide or migrate.

For the first step, corresponding to the growth of the tumors, the following rules apply. At each CA iteration the tumor cells are randomly selected one by one, and a dice is rolled to choose whether each of these cell divides (1), migrates (2), or dies (3).

1. A tumor cell divides with probability

$$P_{div} = 1 - \exp\left(-\frac{(N/T)^2}{\theta_{div}^2}\right). \tag{3}$$

This probability is compared to the probability that results from applying this same formula to a randomly generated number using a normal distribution and the same standard deviation $\theta_{div}/\sqrt{2}$. If the former is greater than the last, division takes place. The higher the value of θ_{div}, the more metabolic requirements for a cell to proliferate. When a cell at position $\vec{x} = (x, y)$ divides, if there are neighboring CA elements that are not currently occupied by tumor cells, we randomly select one $\vec{x'} = (x', y')$ and place there the newborn cell, thus making $T(\vec{x'}) = 1$ and $H(\vec{x'}) = 0$ or $D(\vec{x'}) = 0$, where $D(\vec{x})$ is the function representing the necrotic cells at position $\vec{x}$. However, if all the neighboring elements are occupied, we let the cells pile up, making $T(\vec{x}) \rightarrow T(\vec{x}) + 1$. Concerning the computation of probabilities, some discussion is here deserved. Firstly, we recall that a much more reasonable and simple way that gives very similar results is to generate a random number with uniform distribution between 0 and 1, and to compare P_{div} to the value of that number. This is the standard procedure. The reason why we proceed otherwise in [45–47] is because in [41] it was suggested that the distribution was Gaussian, making us think that N/T had to be considered the random variable. However, the random variable corresponding to every action in a cellular automaton obeys in fact a Bernoulli distribution, since the action takes place or it does not. Then, the particular probability that decides whether this occurs or not depends on the concentration of diffused substances through some function. In particular, here a sigmoid function is used, defined by means of a Gaussian profile. As far as we have investigated, using more simple profiles, as long as they are monotonic, gives very similar results.

2. A tumor cell migrates with probability

$$P_{mig} = 1 - \exp\left(-\frac{(\sqrt{T}M)^2}{\theta_{mig}^2}\right). \tag{4}$$

If P_{mig} is greater than the probability of a randomly generated number, migration proceeds, otherwise it does not. The higher the value of θ_{mig}, the more metabolic requirements for a cell to migrate, unless there are too many tumor cells. When a cell at position $\vec{x}$ moves, if there are neighboring CA elements that are not currently occupied by tumor cells, we randomly select one at $\vec{x'}$ and place the cell there. If there is more than one cell in the original position, the moving cell simply replaces the healthy or the necrotic cell, thus making the transformation $T(\vec{x}) \to T(\vec{x}) - 1$, $T(\vec{x'}) = 1$ and $H(\vec{x'}) = 0$ or $D(\vec{x'}) = 0$.

3. On the other hand, if there is only one tumor cell at $\vec{x}$, then it interchanges its position with the healthy or necrotic cell at $\vec{x'}$. If all the neighboring elements are occupied, we displace the cell to a randomly selected neighboring element.
4. A tumor cell dies with probability

$$P_{nec} = \exp\left(-\frac{(M/T)^2}{\theta_{nec}^2}\right). \tag{5}$$

If P_{nec} is higher than the probability of a randomly generated number, necrosis proceeds, otherwise it does not. The higher the value of θ_{nec}, the greater the probability for a cell to die. When a cell at position $\vec{x}$ dies, we make $T(\vec{x}) \to T(\vec{x}) - 1$. If this is the only cell at $\vec{x}$, then $D(\vec{x}) = 1$.

We now describe the CA rules for the second step, corresponding to the lysis of the tumors. At each CA iteration the immune cells that have one or more tumor cells as first neighbors carry out an attempt to lyse a randomly chosen surrounding tumor cell. This process occurs with probability

$$P_{lys} = 1 - \exp\left(-\frac{1}{\theta_{lys}^2}\left(\sum_{i\in\eta_1} E_i\right)^2\right), \tag{6}$$

where η_n indicates summation up to the n-th nearest neighbors. If P_{lys} is higher than the probability of a randomly generated number, then the selected tumor cell dies. Therefore, $T(\vec{x'}) = 0$, $D(\vec{x'}) = 1$, and the immune cell counter decreases by a unit. If the counter reaches a value of zero, it dies and it is replaced by a healthy cell. The smaller the value of θ_{lys}, the greater the probability for an effector cell to lyse a tumor cell. This parameter was not present in [40] and is introduced here to model the intrinsic cytotoxicity of T cells. When a tumor cell is destroyed by an immune cell, the first neighboring cells are flagged for recruitment. For each CA element without tumor cells a new immune cell is born with probability

$$P_{rec} = \exp\left(-\frac{1}{\theta_{rec}^2}\left(\sum_{i\in\eta_1} T_i\right)^{-2}\right). \tag{7}$$

If P_{rec} is higher than the probability of a randomly generated number, recruitment proceeds. The higher the value of θ_{rec}, the less surrounding tumor cells that are required for T cell recruitment to success. When a cell is recruited at position $\vec{x'}$, we make $D(\vec{x'}) = 0$ or $H(\vec{x'}) = 0$, and $E(\vec{x'}) = 1$.

Those effector cells whose immediate neighborhood is not occupied by tumor cells either migrate or become inactivated. To decide which of these two processes is carried out, a coin is flipped. If the output is migration, it occurs for sure. In the opposite case, inactivation occurs with probability

$$P_{inc} = 1 - \exp\left(-\frac{1}{\theta_{inc}^2}\left(\sum_{i\in\eta_3} T_i\right)^{-2}\right). \tag{8}$$

If P_{inc} is higher than the probability of a randomly generated number, inactivation proceeds. The smaller the value of θ_{inc}, the less surrounding tumor cells that are required for a T cell to become inactivated. When a cell disappears from position $\vec{x}$, we simply make $H(\vec{x}) = 1$ and $E(\vec{x}) = 0$.

2.1.3 The Algorithm

The algorithm starts with a domain full of healthy cells, except for a single tumor cell placed at the center of the domain. Firstly, during this period of growth, each CA step corresponds to 1 day. Every iteration begins with the integration of the reaction–diffusion equations, using a finite-difference scheme and a successive overrelaxation method. Then all the tumor cells are randomly selected with equal probability, and the CA rules are applied. As in previous works [41], every time an action takes place, the reaction–diffusion equations are locally solved in a neighborhood with size 20×20 grid points. Once the tumors have been grown, their dynamics is halted. The immune cells are randomly placed in the vicinity of the tumor and start to evolve. Now the CA step corresponds to 10 min. Firstly, the reaction–diffusion equations are solved and all the immune cells are randomly selected. Then every immune cell is randomly selected and the CA rules are applied. For each immune cell, after applying the CA rules, the nutrients are computed in a local region, in exactly the same manner as before. The algorithm stops when a maximum number of twenty-four steps have been reached, or when the tumor has disappeared.

2.2 An Ordinary Differential Equation Model

In the present investigation the results of the in silico experiments performed with the cellular automaton model are fitted by means of a least-squares fitting method to a Lotka–Volterra type model. The continuous model of cell-mediated immune response to tumor growth consists of three interacting cell populations: the tumor cells $T(t)$, the host healthy cells $H(t)$, and the immune effector cells $E(t)$. Our study focuses mainly on $CD8^+$ T lymphocytes, but the model can be easily modified to reproduce NK cell dynamics. The system of differential equations [35] reads

$$\frac{dT}{dt} = r_1 T\left(1 - \frac{T}{K_1}\right) - a_{12} HT - K(E,T)T \tag{9}$$

$$\frac{dH}{dt} = r_2 H\left(1 - \frac{H}{K_2}\right) - a_{21} TH \tag{10}$$

$$\frac{dE}{dt} = \sigma - d_3 E + g\frac{K^2(E,T)T^2}{h + K^2(E,T)T^2}E - a_{31} TE, \tag{11}$$

with

$$K(E,T) = d\frac{(E/T)^\lambda}{s + (E/T)^\lambda}. \tag{12}$$

The tumor cells and the host healthy cells grow logistically with growth rates and carrying capacities r_1, K_1 and r_2, K_2, respectively. The terms a_{12} and a_{21} model the competition for nutrients and space among tumor and healthy cells. A term representing the fractional cell kill of tumor cells by CTLs is given by the nonlinear function $K(E,T)$, which constitutes the main topic of the present work. Here the parameter σ incorporates a constant input of lymphocytes into the tissue where the tumor develops, but it can be related to a background of NK cells as well [38]. The inactivation of the effector cells and their migration from the tumor area is given by the term $d_3 E$, whereas the parameters g, h stand for the recruitment of immune cells to the tumor domain mediated by cytokines, such as IFN-γ or TNF-α, after the tumor and the immune cells interact. Finally, the competition between the tumor and the T cells for resources is given by a_{31}. These differential equations are solved using a fourth order Runge–Kutta integrator.

This continuous model has been validated [35] using experiments from [36] and the parameter values are listed in Table 1. In the present work only those parameters appearing in the fractional cell kill (d, λ, and s) are inspected. Accordingly to the CA model, we have set $\sigma = 0$ in the ODE model since the CA does not include a constant input of effector cells. We have also selected a value $g = 0.15$, which is very close to one of the values appearing in Table 1. Importantly the CA model and the ODE model include the same type of processes. The logistic growth of tumor cells in the CA model arises as a consequence of competition for nutrients [41].

Table 1 The values of the parameters in the ordinary differential equation model used to fit experiments from [36]

Parameter	Units	Value	Description
r_1	day^{-1}	5.14×10^{-1}	Tumor cells growth rate
K_1	cell	9.8×10^{8}	Tumor carrying capacity
a_{12}	cell $^{-1}$ day $^{-1}$	1.1×10^{-10}	Competition of host cells with tumor cells
$d(nn)$	day^{-1}	2.20	Saturation level of fractional tumor cell kill
$d(nl)$		3.47	
$d(ln)$		2.60	
$d(ll)$		7.86	
$s(nn)$	None	1.6	Steepness coefficient of fractional tumor cell kill
$s(nl)$		2.5	
$s(ln)$		1.4×10^{-1}	
$s(ll)$		4.0×10^{-1}	
$\lambda(nn)$	None	1.2×10^{-1}	Exponent of fractional tumor cell kill
$\lambda(nl)$		2.1×10^{-1}	
$\lambda(ln)$		7.0×10^{-1}	
$\lambda(ll)$		7.0×10^{-1}	
r_2	day^{-1}	1.80×10^{-1}	Host cells growth rate
K_2	cell	1.0×10^{9}	Host cells carrying capacity
a_{21}	cell $^{-1}$ day $^{-1}$	4.8×10^{-10}	Competition of tumor cells with host cells
σ	cells day^{-1}	7.5×10^{4}	Constant source of effector cells
d_3	day^{-1}	6.12×10^{-2}	Inactivation rate of effector cells
$g(nn)$	day^{-1}	3.75×10^{-2}	Maximum recruitment rate
$g(nl)$		3.75×10^{-2}	
$g(ln)$		1.13×10^{-1}	
$g(ll)$		3.00×10^{-1}	
h	cell^2	2.02×10^{7}	Steepness coefficient for the recruitment
a_{31}	cell $^{-1}$ day $^{-1}$	2.8×10^{-9}	Immune–tumor competition

The parenthesis represents four different cases: a primary challenge with control-transduced cells followed by a secondary one with ligand (*nl*) or control (*nn*) cells, and a primary interaction with ligand-transduced cells followed again by ligand (*ll*) or ligand-negative (*ln*) rechallenges

There is also competition among healthy cells and tumor cells for nutrients, which in the ODE model is represented by the competing Lotka–Volterra terms between healthy and tumor cells. T cell lysis, inactivation, and recruitment are also present in both models. Only the competition term between tumor and immune cells a_{31} is different. Although we keep this parameter as shown in Table 1, if desired, it can be made equal to zero. As far as we have investigated, reducing the value of this parameter produces no appreciable consequences in our study. Notwithstanding this correspondence, we recall that during the second step of our CA simulations, the tumor dynamics is suspended. Accordingly, the parameter r_1 should be made equal to zero. Again, we keep this parameter as shown in Table 1. Reducing the value of this parameter produces no significant consequences in our study when the T cells

are effective, because the time scale of T cell lysis (less than 1 h) is considerably smaller that the time scale of cell division (around 1 day). For immunodeficient scenarios the effects are more sensitive, but still small. In other words, T cell dynamics dominates during the first 4 h.

3 The Lysis of Tumors in the Absence of Growth

3.1 Tumors

In Fig. 2 we depict the simulated solid tumors with four distinct morphologies, depending on the nutrient competition among tumor cells. The apparent three-dimensionality is an artifact resulting from the fact that we let cells pile up at the CA grid points. This piling mechanism was assumed in [41] for computational simplicity, and does not have any consequence in our study, since once the tumors

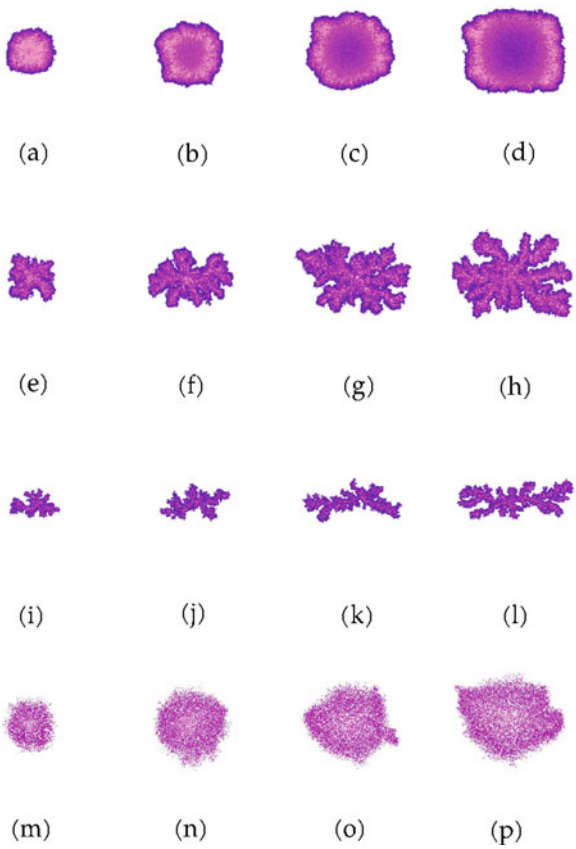

Fig. 2 Tumors generated using the cellular automaton model. Tumors become increasingly branchy as the competition for nutrients increases. Colors go from dark purple (one cell) to light pink (highest number of cells in a grid point for each tumor). We set the parameters $\lambda_M = 10$ and $\theta_{nec} = 0$ in all the cases, disregarding necrosis. (**a**)–(**d**) Spherical tumors with increasing size and parameters $\alpha = 2/n$, $\lambda_N = 25$, $\theta_{div} = 0.3$, and $\theta_{mig} = \infty$. (**e**)–(**h**) Papillary tumors with increasing size and parameters $\alpha = 4/n$, $\lambda_N = 200$, $\theta_{div} = 0.3$, and $\theta_{mig} = \infty$. (**i**)–(**l**) Filamentary tumors with increasing size and parameters $\alpha = 8/n$, $\lambda_N = 270$, $\theta_{div} = 0.3$, and $\theta_{mig} = \infty$. (**m**)–(**p**) Disconnected tumors with increasing size and parameters $\alpha = 3/n$, $\lambda_N = 200$, $\theta_{div} = 0.75$, and $\theta_{mig} = 0.02$

are grown, we project them to study their lysis. High values of α and λ_N lead to more branchy tumors, gradually changing from spherical to filamentary. This break of the spherical symmetry of the tumors is explained if we consider that when some nearby neoplastic cells on the boundary of a tumor compete aggressively for nutrients, those cells that divide and take ahead at some step preserve this advantage at the next step, stealing the nutrients to those cells left behind. The four geometries are comparable to a variety of histologies [41], such as a basal cell carcinoma, a squamous papilloma, a trichoblastoma, and a plasmacytoma. Note that the necrosis of tumor cells due to the scarcity of nutrients in the core of the masses has been neglected, since it has no relevance in our study. In the CA this is achieved by setting $\theta_{nec} = 0.01$ for all our simulations. Except for the disconnected patterns appearing in the last row in Fig. 2, motility has been also disregarded, considering sufficiently high values of θ_{mig}.

3.2 *Effective Immune Response*

In the model given by Eqs. (9)–(11), the fractional cell kill of tumor cells by CTLs is given by the function $K(E, T)$. In [35] we opted for expressing this function in the form

$$K(E, T) = d\frac{E^{\lambda}}{h(T) + E^{\lambda}}, \tag{13}$$

with $h(T) = sT^{\lambda}$. Written this way, the fractional cell kill clearly states that the more the effector cells, the greater the fractional cell kill, but bearing in mind the saturation of antigen-mediated immune response, which depends on the tumor burden. We propose that the saturation is due to the crowding of immune effector cells, which is evident if we recall that these cells need to be in contact with tumor cells to exterminate them. In a solid tumor, once all the tumor cells on its surface are in contact with a first line of immune cells, the remaining effector cells are not lysing, although the adjacent lines behind probably contribute to immune stimulation through several feedback mechanisms. Therefore, at a certain point, no matter how many more immune cells are present in the region of interest, the rate at which the tumor is lysed remains practically unaltered. Before saturation appears, if two tumors of the same nature and different size at a certain time instant are lysed at the same rate by the immune system, the bigger tumor will require more effector cells. Put more simply, if two tumors of different size are reduced to a particular fraction of its size after a certain period of time, the bigger tumor will require more effector cells. The number of effector cells E for which the fractional tumor cell kill is half of its maximum d increases monotonically with the tumor size $h(T)$.

We use simulations to demonstrate that these assertions are sufficient to explain the fractional cell kill law, even though there might be others. With this purpose, for every tumor pictured in the previous section, we prepare co-cultures with different effector-to-target ratios. Then, we let the CA evolve and measure the lysis 4 h later (see Fig. 3). As previously explained, the tumors have been projected before the lysis starts, to better correlate the geometry and the parameters in the fractional cell kill. Otherwise, we would have two-dimensionally distributed lymphocytes fighting three-dimensional-like tumors, since in our CA we do not let the immune cells pile up. We do it this way to avoid the unfair situation in which just a few immune cells

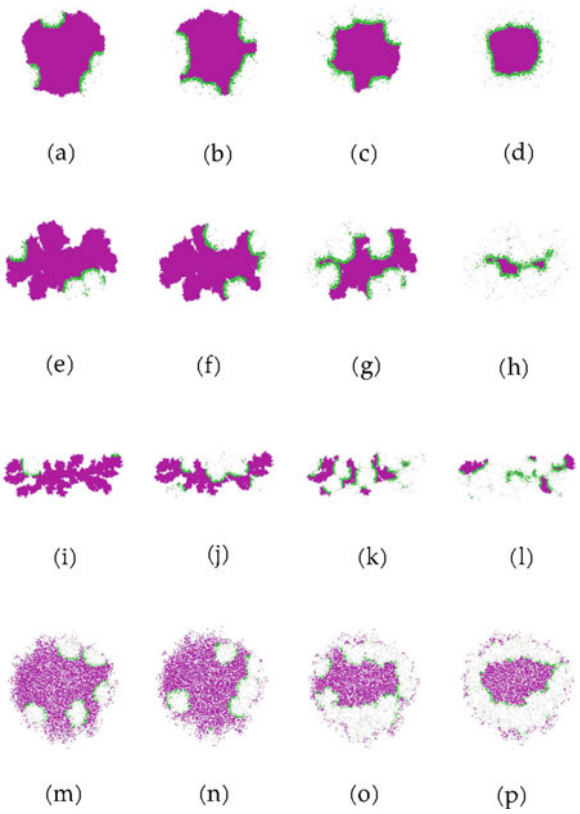

Fig. 3 Lysed tumors after 4 h for different effector-to-target ratios. The effector cells (green) form satellites that advance destroying their neoplastic enemies (violet) and leave apoptotic bodies (light gray) behind them. The parameter values of the CA are $\theta_{lys} = 0.3$, $\theta_{rec} = 1.0$, $\theta_{inc} = 0.5$, $\lambda_M = 10$, $\lambda_N = 25$, and $\alpha = 2/L$. (**a**)–(**d**) Spherical tumor in Fig. 2b with E_0/T_0 taking values on the set {0.0025, 0.005, 0.05, 0.75}, respectively. (**e**)–(**h**) Papillary tumor in Fig. 2f with E_0/T_0 taking values on the set {0.005, 0.0075, 0.025, 0.25}, respectively. (**i**)–(**l**) Filamentary tumor in Fig. 2l with E_0/T_0 taking values on the set {0.0025, 0.0075, 0.017, 0.025}, respectively. (**m**)–(**p**) Disconnected tumor in Fig. 2n with E_0/T_0 taking values on the set {0.005, 0.0075, 0.015, 0.025}, respectively

are facing a big pile of tumor cells, and vice versa. Finally, the results are fitted to the ODE model using a least-squares fitting method. We recall that such model was validated using as initial conditions typical cell populations of 10^6 cells, while the CA automaton grid used can harbor at most 9×10^4 cells. However, this is not a hurdle at all, since if desired, the cell populations in the ODE model can be renormalized and its parameters redefined so as the cell numbers coincide.

The resulting lysis curves are depicted in Fig. 4 and the values of the parameters d, λ, and s in Eq. (13) are listed in Table 2, together with the fractal dimension D_F of the boundary of the initial tumors. Satellitosis is clearly appreciated as a consequence of T cell recruitment, and the resulting clusters of cells act like wave fronts that advance lysing the tumor. Note that the immune cells that are far enough from the tumor become inactivated after several iterations of the CA. Consequently, only the T cells that are able to make contact with the tumor, gain traction in killing and subsequent recruitment, appear in the figures. There is a correlation between the box-counting dimension and the parameters d and λ for the connected tumors examined, but this is not case for the disconnected one. The disconnected tumors shown in Fig. 2 display the highest box-counting dimension, because they are very drilled, so that most of the tumor cells are on its boundary. However, they are rather spherical, and for this reason the part of the boundary that is in the center of the mass is not initially accessible to the immune cells. These facts explain the low values of d and λ for such tumors, which are comparable to the spherical ones. Therefore, in our model, those tumors with a bigger surface of contact are lysed faster. Indeed, what matters to the cytotoxic cells is how accessible their enemies are. The more the tumor cells there are between an immune cell and some other tumor cell, the

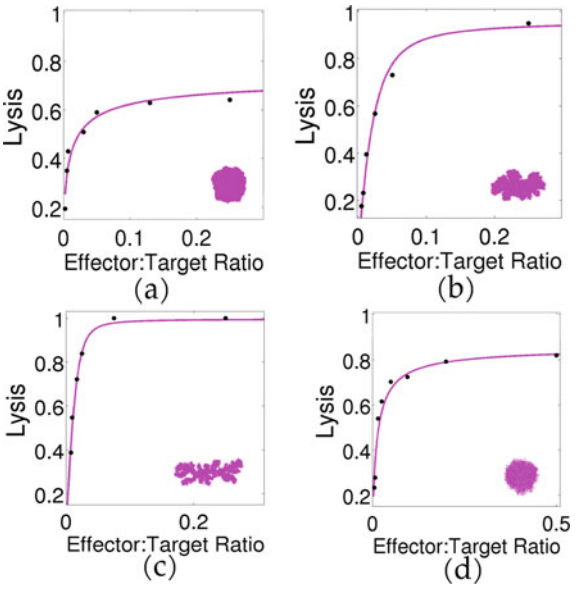

Fig. 4 The lysis of tumor cells after 4 h versus the effector-to-target ratio E_0/T_0 in immunocompetent environments. The parameter values of the CA related to the lysis, recruitment, and inactivation are $\theta_{lys} = 0.3$, $\theta_{rec} = 1.0$, and $\theta_{inc} = 0.5$, respectively. The solid curve corresponds to the ODE model, while the points correspond to the cellular automaton results. (**a**) The spherical tumor in Fig. 2b. (**b**) The papillary tumor in Fig. 2f. (**c**) The filamentary tumor in Fig. 2l. (**d**) The disconnected tumor in Fig. 2n

Table 2 The parameter values modified in the model shown in Eqs. (9)–(11) corresponding to an effective immune response

Parameter	Units	Value	Description
d(s)	day^{-1}	9 ± 4	Saturation level of fractional tumor cell kill
d(p)		20 ± 1	
d(f)		32 ± 2	
d(d)		13 ± 3	
λ(s)	None	0.61 ± 0.07	Exponent of fractional tumor cell kill
λ(p)		0.87 ± 0.04	
λ(f)		0.89 ± 0.03	
λ(d)		0.63 ± 0.03	
s	None	0.15	Steepness coefficient of fractional tumor cell kill
D_F(s)	None	1.09 ± 0.02	Box-counting dimension of the boundary before the lysis starts
D_F(p)		1.21 ± 0.04	
D_F(f)		1.36 ± 0.02	
D_F(d)		1.72 ± 0.04	

The parameters λ and d are obtained through a least-square fitting of the lysis of tumor cells between the CA simulations and the ODE model. The mean value and standard deviations are computed for each morphology using four different tumors sizes: spherical (s), papillary (p), filamentary (f), and disconnected (d)

lower the rate at which the effector cells kill their victims. This is starkly evident for the spherical tumors, which correspond to the smallest values of d and λ.

Thus, according to our model, Eq. (13) is a robust emergent property of the tumor–immune interaction depending on the spatial distribution of the tumor cells. It reflects the saturation of an effective immune system, which depends on the tumor size. This saturation is fruit of the crowding of the effector cells and the arduousness to establish contact with their adversaries. Nevertheless, it takes hours for the effector cells to fully lyse the tumors so far investigated, which denotes that this extrinsic limitation to the lytic capacity of the immune system is barely important compared to the immunoevasive maneuvers that tumor cells commonly orchestrate [1].

3.3 Ineffective Immune Response

Tumor cells find ways to evade the immune surveillance through a broad range of mechanisms [48]. They can acquire the ability to repress tumor antigens, MHC class I proteins, or NKG2D ligands. They may also learn to destroy receptors or to saturate them, induce suppressor T cells formation, launch counterattacks against immunocytes by releasing cytokines, avoid apoptosis, etc. It is therefore pertinent

to ask ourselves if the fractional cell kill can cover situations in which the tumor microenvironment is immunodeficient.

In [38] the authors show that the lysis curves corresponding to NK cells in the experiments borrowed from [36] do not show saturation, and that a fractional cell kill given by a simple power law cE^{ν} works to fit such data. Because much higher values of the effector-to-target ratio are required to obtain similar values for the lysis compared to the CTLs curves, it was suggested that when the effector cells are less effective, saturation is not observed.

Mathematical arguments have been given [35] to explain this lack of saturation. Briefly, when the cytotoxic cells are less effective, only a fraction f of the effector cells are interacting with the tumor. Thus we can replace E by fE in the fractional cell kill. Now, defining $\tilde{s} = s/f^{\lambda}$, the fractional cell kill law remains unchanged. This suggests that the parameter s is related to the effectiveness of the cytotoxic cells, being this parameter inversely proportional to the effectiveness of such cells. On the other hand, if the effectiveness is small enough ($f \ll 1$), then $h(T)$ dominates over E^{λ} in Eq. (13), as long as E is not too high. The resulting lysis term becomes $df^{\lambda}E^{\lambda}T^{1-\lambda}/s$. This facts legitimize the estimation $cE^{\nu}T$ that has been used in other works [35, 38] to reproduce the fractional cell kill of tumor cells. Nevertheless, here we do not want to introduce phenomenological functions of this type, but rather concentrate our efforts on the significance of s. To this end, we diminish the intrinsic cytotoxic capacity of the immune cells, which is encoded in the parameter θ_{lys} in our cellular automaton. Higher values of this parameter represent more ineffective T cells. The results can be seen in Fig. 5 and the values of the parameters are listed in Table 3. As we increase the parameter θ_{lys}, the saturation appearing in the lysis curves becomes less evident, and at a certain point it disappears.

When $\theta_{lys} = 10$, the ODE model can be adjusted to the CA results. However, increasing s is not sufficient to reproduce this data, and considerable variations of

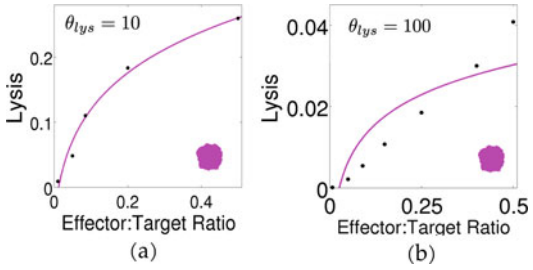

Fig. 5 The lysis of tumor cells after 4 h versus the effector-to-target ratio E_0/T_0 in immunosuppressed environments. The spherical tumor represented in Fig. 2b is studied, with recruitment and inactivation CA parameters $\theta_{rec} = 1.0$ and $\theta_{inc} = 0.5$. The solid curve corresponds to the ODE model, while the points correspond to the cellular automaton results. (**a**) A more ineffective, but still effective, adaptive response is here represented, with $\theta_{lys} = 10$. (**b**) A value of the intrinsic cytotoxic capacity $\theta_{lys} = 100$ is set for the most ineffective immune system

Table 3 The parameter values of the fractional cell kill given by Eq. (13)

Parameter	Units	Value	Description
d(s)	day^{-1}	3.80	Saturation level of the fractional tumor cell kill
d(i)		1.56	
λ(s)	None	0.62	Exponent of the fractional tumor cell kill
λ(i)		0.17	
s(s)	None	0.50	Steepness coefficient of the fractional tumor cell kill
s(i)		1.10	

These parameters are obtained through a least-square fitting of the lysis of tumor cells between the CA simulations and the ODE model (see Fig. 5). Two cases are represented: a very ineffective (i) and a semi-effective (s) immune responses

the remaining parameters d and λ are required. A much more dramatic case arises when $\theta_{lys} = 100$. In this case we have not been able to find any values of the parameters that represent faithfully the CA results. The best fitting provided by the ODE model exhibits considerable saturation. The conclusion is that the fractional cell kill represented by Eq. (13) works bad for immunodeficient environments and also confuses the geometrical effects and the intrinsic cytotoxic capacity of the immune cells. In the next section, we propose a new fractional cell kill that allows to fit the results more accurately by simply reducing the value of s.

3.4 Modification of the Fractional Cell Kill

In [35], the particular nature of the function $h(T)$ appearing in Eq. (13) was also discussed, proving that if instead of $h(T) = sT^{\lambda}$, $h(T) = sT^{\lambda+\Delta\lambda}$ is used, the empirical results can also be validated by simply decreasing the value of s, even for values $\Delta\lambda/\lambda$ greater that one. This means that the original proposal of a saturating fractional cell kill depending on the quotient E/T cannot be guaranteed.

Furthermore, from a theoretical point of view, the function $h(T) = sT^{\lambda}$ makes the model ill-defined in the limit of very big tumors ($T \to \infty$) facing a comparably small fixed number of immune cells. The reason is that in this limit we get unbounded velocity for the lysis ($K(E, T)T \to \infty$). We demonstrate that $h(T) = sT$ is a much better choice. It has been shown [44, 49] that for a fixed number of effector cells E_0, the Michaelis–Menten kinetics govern the lysis of tumor cells. The value of the lytic velocity at tumor saturation, i.e., when $T \to \infty$, is reported in such works as a measure of the intrinsic cytotoxic capability of a particular number of effector cells. A Michaelis–Menten decay in Eq. (13) is obtained for a constant value of effector cells as long as $h(T) = sT$ is used. The value at saturation for a fixed number of effector cells is then dE_0^{λ}/s. An argument supporting saturation comes from the following fact. If the number of tumor cells is much higher than

a fixed number of effector cells, the velocity at which the tumor cells are lysed cannot be enhanced by increasing the number of the neoplastic cells. This occurs because T cells kill tumor cells one by one, and for such ratios all the effector cells are already busy fighting other cells. In a similar fashion, for an enzymatic reaction, one cannot increase arbitrarily the velocity at which the products are formed by simply adding more substrate. Precisely, this reasoning is reminiscent of the original formulation proposed by [31], in which the cell populations are regarded as chemical species obeying enzymatic kinetics in the quasi-steady state regime. In such work, the tumor cells are the substrate, the effector cells are the enzyme, and the products are the dead cells. Indeed, in the following section we use enzyme kinetics as a metalanguage to provide an analytical derivation of the fractional cell kill. A fractional cell kill function that yields bounded velocity for the lysis of tumor cells when any of these two cell populations is sufficiently high compared to the other is represented by

$$K(E,T) = d\frac{E^{\lambda}}{sT + E^{\lambda}}. \tag{14}$$

If we focus only on the lysis of tumor cells, the velocity at which the tumor is reduced can be represented by the following nonlinear differential equation:

$$\dot{T} = -d\frac{E^{\lambda}}{sT + E^{\lambda}}T. \tag{15}$$

Following the point of view of [31], this mathematical expression can be regarded as a Michaelis–Menten kinetics where the rate constants of the formation of the "enzyme–substrate" conjugates, their dissociation and their conversion to product depend nonlinearly (as power laws) on the enzyme concentration. It establishes the saturation of the velocity of the lysis of tumor cells for both the tumor and the immune cell populations. In Fig. 6a we first reproduce the experiments of the spherical tumor shown in Fig. 2b for $\theta_{lys} = 0.3$. This allows us to obtain the parameter values of the modified fractional cell kill shown in Eq. (14). Then we carry out the simulations of the preceding section for immunodeficient environments and see how, mainly by increasing the value of s, the CA results are reproduced (see Fig. 6b, c). The parameter values are listed in Table 4. This sheds light into the significance of this parameter, which is now manifestly related to the intrinsic cytotoxic potential of the T cells. Moreover, this implies that the limit $T \to \infty$, for which the quantity dE^{λ}/s is obtained, is not a good measure of lymphocyte cytotoxicity, as suggested in [44, 49]. This limit, which for a constant value of the T cells implies a linear decay of the tumor, involves geometry as well. Ideally, if we consider that there is just one immune cell, and it takes this cell 1 h to lyse one tumor cell, then a spherical tumor would be reduced at approximately one cell per hour (assuming that this immune cell does not become inactivated at some step). However, the geometry of the tumor, which is coded in the parameters d and λ, clearly affects how fast this single cell can erase it.

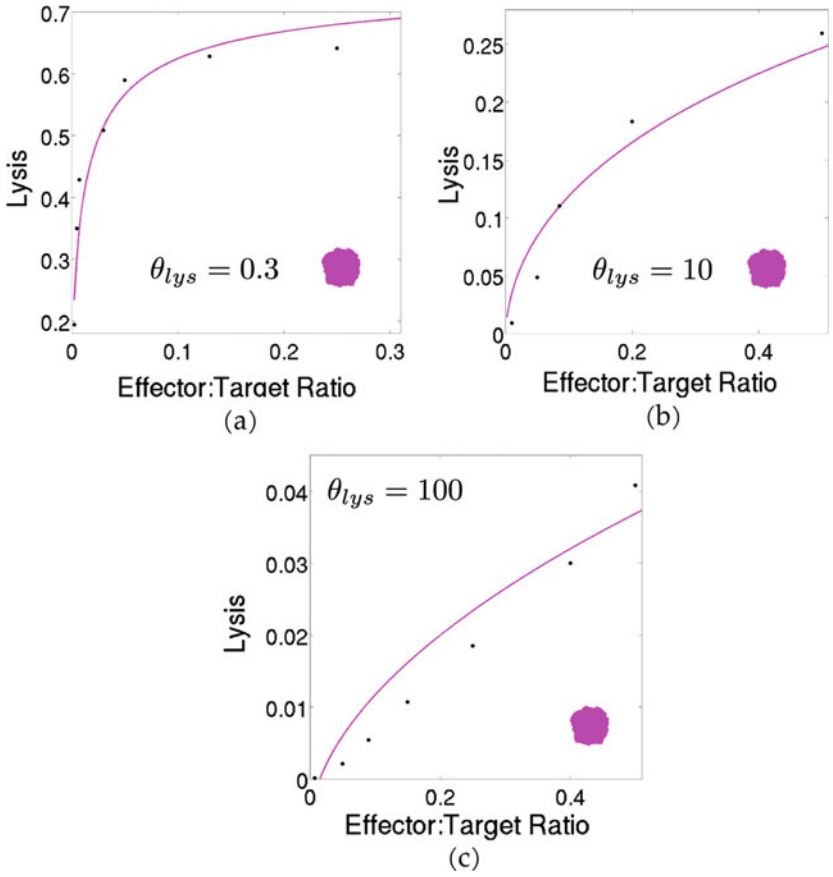

Fig. 6 The lysis of tumor cells after 4 h versus the effector-to-target ratio E_0/T_0 for increasing ineffectiveness of the lymphocytes. The spherical tumor represented in Fig. 2b is studied, with recruitment and inactivation CA parameters $\theta_{rec} = 1.0$ and $\theta_{inc} = 0.5$. The solid curve corresponds to the ODE model, while the points correspond to the cellular automaton results. (**a**) An effective immune response for $\theta_{lys} = 0.3$. (**b**) A more ineffective, but still effective, adaptive response is here represented, with $\theta_{lys} = 10$. (**c**) A value of the intrinsic cytotoxic capacity $\theta_{lys} = 100$ is set for the most ineffective immune system. As shown in Table 4, the intrinsic cytotoxic potential of the T cells is chiefly represented by parameter s in Eq. (14)

Even though the reduction of saturation for ordinary values of the effector-to-target ratio can be justified mathematically and numerically, the change in curvature for the CA results appearing in Fig. 6c requires a positive feedback mechanism. Certainly, the mechanism responsible for this phenomenon is the recruitment of immune cells, which becomes increasingly important as the effectiveness of the T cells decreases.

Table 4 The parameter values of the fractional cell kill appearing in Eq. (14)

Parameter	Units	Value	Description
d(e)	day^{-1}	9.22	Saturation level of the fractional tumor cell kill
d(s)		9.62	
d(i)		9.52	
λ(e)	None	0.50	Exponent of the fractional tumor cell kill
λ(s)		0.51	
λ(i)		0.55	
s(e)	cells$^{\lambda-1}$	1.0×10^{-5}	Steepness coefficient of the fractional tumor cell kill
s(s)		1.4×10^{-4}	
s(i)		9.5×10^{-4}	

These parameters are obtained through a least-square fitting of the lysis of tumor cells between the CA simulations and the ODE model (see Fig. 6). Three cases are represented: an effective (e), a semi-effective (s), and ineffective immune responses (i). Note that it is only the parameter s, which is related to the intrinsic cytotoxic capacity, that varies substantially. It increases as the immune cells become less effective

4 The Fractional Cell Kill as a Michaelis–Menten Kinetics

The fractional cell kill represented by Eq. (14) can be derived from the Michaelis–Menten kinetics [27, 28] assuming that the rate constants of the reaction depend on the enzyme concentration. During the process of lysis, the effector cells E bound to the tumor cells T forming complexes C, and dead tumor cells T^* result from this interaction. Therefore, the tumor cells play the role of the substrate and the effector cells act as the enzyme. This cellular reaction can be written in the form

$$E + T \underset{k_{-1}}{\overset{k_1}{\rightleftharpoons}} C \underset{k_{-2}}{\overset{k_2}{\rightleftharpoons}} T^* + E. \tag{16}$$

Once a tumor cell is induced to apoptosis it cannot resurrect, so we must set $k_{-2} = 0$. Generally, also the backward reaction represented by k_{-1} should be disregarded, since after tumor cell recognition and complex formation, destruction proceeds. However, we keep this term for reasons explained below.

Assuming that the law of mass action holds, the system of differential equations governing the reactions is

$$\frac{dE}{dt} = -k_1 ET + (k_{-1} + k_2)C \tag{17}$$

$$\frac{dT}{dt} = -k_1 ET + k_{-1} C \tag{18}$$

$$\frac{dC}{dt} = k_1 ET - (k_{-1} + k_2)C \tag{19}$$

$$\frac{dT^*}{dt} = k_2 C. \tag{20}$$

The Briggs–Haldane [50] quasi-steady state approximation $\dot{C} = 0$ was assumed in [31] because in their model the time scale of the process of lysis is considerably smaller than that of cell growth. However, if we focus on the process of lysis only, the quasi-steady state approximation requires

$$\frac{E_0}{T_0 + K_M} \ll 1, \tag{21}$$

where $K_M = (k_{-1} + k_2)/k_1$ is the Michaelis constant, and E_0 and T_0 are the initial concentrations of the effector and the tumor cells, respectively.

Because we are dealing with situations in which the substrate concentration can be smaller than the enzyme, the quasi-steady state approximation implies $K_M \gg E_0$. Since this condition cannot be generally guaranteed, instead, we consider Michaelis and Menten original formulation, and suppose that the substrate is in instantaneous equilibrium with the complex. We believe this is more reasonable, because it takes about 1 h for a cytotoxic T cell to fully lyse one tumor cell and, if the cells are effective, the recognition and complex formation should occur quite fast when brought together. In this manner, we have $k_1 ET = k_{-1} C$. From Eqs. (17) and (19) we get the conservation law $E + C = E_0$. These two equations put together and substituted in Eq. (20) yield

$$\frac{dT^*}{dt} = k_2 k_1 E_0 \frac{T}{k_1 T + k_{-1}}. \tag{22}$$

So far, this is nothing else but the Michaelis–Menten kinetics. It is at this point that we have to consider a dependence of the rate constants of the reaction on the concentration of the effector cells. The mathematical relations are derived heuristically, based on the idea that for higher concentrations of the immune cells the rate constants vary in such a manner that the whole process is pushed backwards. Since saturation is due to the crowding of T cells, and this depends on the geometry of the tumor, it seems a natural choice to use power laws.

Once the first lines of effector cells cover the surface of a solid tumor, the remaining immune cells are not in contact with it. Alternatively, an equivalent argument is attained if we suppose that the non-interacting effector cells do interact with some tumor cells unsuccessfully (say ghost tumor cells), so that the complexes are dissociated without lysis. The more the effector cells, the higher the rate of dissociation, and when the number of effector cells is small compared to the number of tumor cells, the dissociation should vanish. Therefore, we consider a power law dependence $k_{-1}(E_0) = \kappa_{-1} E_0^{\alpha}$, with $0 < \alpha < 1$, as suggested from the experiments. Substitution in Eq. (22) yields

$$\frac{dT^*}{dt} = k_2 k_1 \frac{E_0}{k_1 T + \kappa_{-1} E_0^{\alpha}} T. \tag{23}$$

The fractional cell production of dead cells in this equation already resembles very much to Eq. (14). To obtain the exact result we have to consider dependence of k_1 and k_2 on the effector concentration as well. Note that for the inverse reaction to take place complexes have to be formed first, and this requires some time. Therefore, saying that complexes dissociate without lysis is not exactly equivalent to stating that the complexes are not formed. These rates should decay for increasing concentrations of the effector cells, diminishing the rate of formation of complexes and products. Once again, we postulate power law relations in the form $k_1(E_0) = \kappa_1 E_0^{-\beta}$ and $k_2(E_0) = \kappa_2 E_0^{-\gamma}$, where again $0 < \beta < 1$ and $0 < \gamma < 1$. It might result surprising that in the limit $E_0 \to \infty$ these functional relations tend to zero, suggesting that the reaction stops. However, this is not the case, because when substituted in Eqs. (17)–(20), $k_1(E)E$ and $k_2(E)C$ both increase with the number of effector cells. Replacing the rate functions in Eq. (23) we obtain

$$\frac{dT^*}{dt} = \frac{\kappa_1\kappa_2}{\kappa_{-1}} \frac{E_0^{1-\gamma}}{\frac{\kappa_1}{\kappa_{-1}} T + E_0^{\alpha+\beta}} T. \tag{24}$$

We now rename the constants $\lambda = \alpha + \beta$, $s = \kappa_1/\kappa_{-1}$, $d = \kappa_1\kappa_2/\kappa_{-1}$, and remember that the velocity for the lysis must remain bounded for $E_0 \to \infty$, which imposes the constraint $\alpha + \beta + \gamma = 1$. Thus, the velocity at which dead tumor cells accumulate is given by the nonlinear function

$$\frac{dT^*}{dt} = d \frac{E_0^{\lambda}}{sT + E_0^{\lambda}} T. \tag{25}$$

5 Decay Laws in Tumor Cell Lysis

Using the Michaelis–Menten kinetics as the modelling framework describing tumor–immune interactions at the cellular scale [31], a mathematical expression describing the velocity at which a population of cytotoxic cells lyse a tumor has been derived in the previous sections. A schematic representation of such a cellular reaction is seen in Fig. 7. When a T cell identifies a tumor cell through the recognition of antigens, these two cells form complexes. As a result, apoptosis is induced and a dead tumor cell is produced. However, some of the assumptions that lead to the Michaelis–Menten kinetics, such as a high substrate concentration compared to the enzyme concentration, or high values of the Michaelis constant compared to the enzyme concentration, are not met in the present case. To reproduce experiments, the constant rates of the reaction require dependence on the number of effector cells, in such a manner that saturation of the velocity is also found for increasing numbers of the effector cells. As previously stated, saturation occurs in both directions. Disregarding other processes, the differential equation [46]

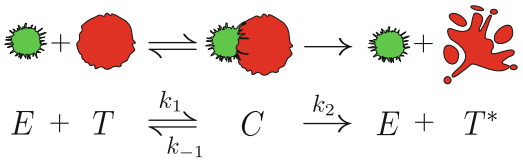

Fig. 7 The cell-mediated immune response as an enzymatic reaction. An interaction between an activated lymphocyte E, colored in green, and a tumor cell T, painted in red. When the lymphocyte identifies the tumor cell these two cells form a complex. The result of the interaction is the initial T cell and an apoptotic tumor cell T^*. This cellular interaction is similar to an enzymatic chemical reaction, where the tumor cell plays the role of the substrate and the T cell acts as an enzyme (figure obtained from Ref. [45])

describing the velocity at which the tumor cells are destroyed is $\dot{T} = -K(E,T)T$, with $K(E,T)$ the fractional cell kill, which can be written as

$$K(E,T) = d\frac{E^{\lambda}}{sT + E^{\lambda}}, \tag{26}$$

where T and E represent the number of tumor cells and immune cells, respectively. The parameters d and λ depend on the tumor geometry. Less spherical tumors lead to higher values of these parameters. On the other hand, the parameter s is related to the intrinsic ability of the cytotoxic cells to recognize and destroy their adversaries. Smaller values of this parameter are related to more effective immune cells. Thus, the velocity at which a tumor is lysed is given by

$$\dot{T} = -d\frac{E^{\lambda}}{sT + E^{\lambda}}T. \tag{27}$$

In the present section we delve deeper into the significance of this mathematical expression by examining the different limits that it provides. To reproduce also the time series as well as the lysis curves, we introduce one last rearrangement.

5.1 The Limits of the Fractional Cell Kill

We begin by carefully examining the different limits that this equation possesses (see Fig. 8). For a fixed number of immune cells E_0, when the immune cell population is small compared to the tumor size ($E_0^{\lambda} \ll sT$), the tumor cell population is reduced at a constant velocity

$$\dot{T} = -dE_0^{\lambda}/s. \tag{28}$$

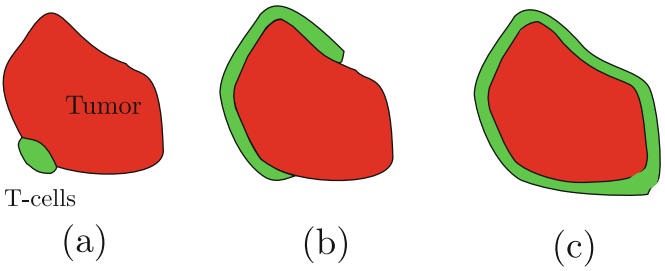

Fig. 8 The limits of the fractional cell kill in the absence of T-cell infiltration. (**a**) A small immune cell population facing a big tumor. In this limiting situation the decay of the tumor is rather linear, as shown in Eq. (28). (**b**) The intermediate case in which a considerable part of the tumor is covered with immune cells. (**c**) A tumor, in which surface is totally covered with immune cells. In this extreme case the velocity of the decay can be approximated by a parabolic decay, as shown in Eq. (31) (figure obtained from Ref. [45])

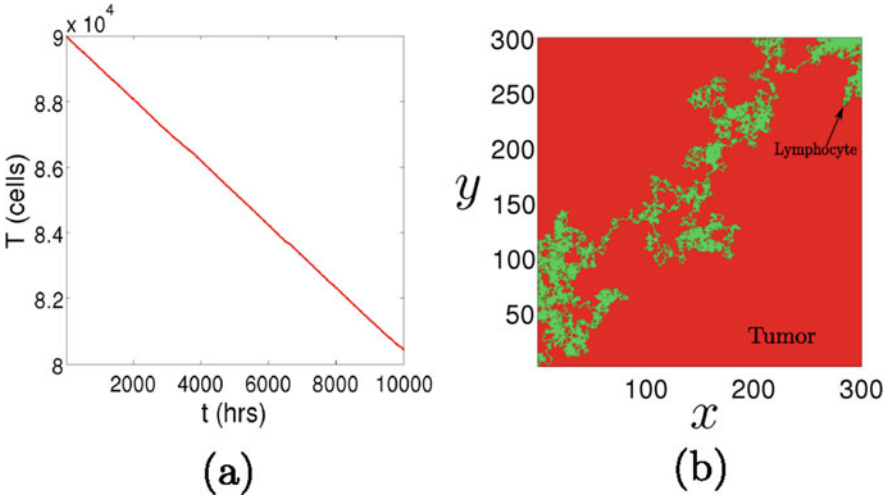

Fig. 9 A single cell lysing a tumor. (**a**) The linear decay of a tumor in the limit in which there is only one immune cell. (**b**) The path (green) of a lymphocyte after a certain time, modelled by an unbiased random walk in a square domain, which is occupied by tumor cells (red). The initial condition is set on the left bottom corner (figure obtained from Ref. [45])

This *linear decay* makes perfect sense if we bear in mind the extreme situation in which there is only one lymphocyte fighting a tumor of a certain size. Ideally, if it takes the immune cell approximately 1 h to lyse a tumor cell, then the velocity of the decay is simply one tumor cell per hour. Even though this is fairly obvious, in Fig. 9 we show the random walk of a lymphocyte lysing a tumor that occupies a square domain, at one cell per hour. In practice, the velocity clearly depends on the intrinsic ability of the cytotoxic cell s to lyse the tumor cells and also on the tumor morphology λ and d. On the other hand, when the immune cell population is

high enough compared to the tumor cell population ($E_0^{\lambda} \gg sT$), Eq. (27) yields an *exponential decay*

$$\dot{T} = -dT. \tag{29}$$

Now, the scenario corresponds to the case in which the tumor is totally covered with effector cells. For the sake of simplicity, we consider a tumor spheroid [51]. At each step the immune cells lyse a layer of tumor cells, and the radius of the spheroid decreases. In the next round another layer is eliminated but, since the tumor has smaller radius, so it does the length of this second layer. Therefore, the velocity decreases as the tumor is gradually erased. Nevertheless, note that for a three-dimensional solid tumor the reduction occurs in surface, while the tumor is distributed in volume, suggesting that the decay should be slower than exponential.

It has been demonstrated [46] that Eq. (27) reproduces accurately the values of the lysis after some fixed time versus different values of the effector-to-target ratio as initial conditions. However, here we show that it is unable to reproduce the time series of the tumor decay faithfully. A more general mathematical function which is better at reproducing the time series of the tumor decay can be derived in the following manner. Assume that a two-dimensional tumor with the shape of a disk is plainly covered with immune cells. As shown in Fig. 10a, a layer of tumor cells is erased by the immune cells at each step, like peeling an onion. If we write the radius of the disk at the n-th step as R_n, and the diameter of a cell as ΔR, the dynamics of the tumor can be represented by a very simple map in the form $R_{n+1} = R_n - \Delta R$. Since the area of a disk is related to the radius through $A = \pi R^2$, a direct substitution yields the map $A_{n+1} = A_n + \pi \Delta R^2 - 2\pi^{1/2} \Delta R A_n^{1/2}$, where A_n is the area of the disk at the n-th step. If we consider that the immune cells lyse at a constant rate, then $\Delta R = c\Delta t$, and we obtain

$$\frac{\Delta A_n}{\Delta t} = \pi c^2 \Delta t - 2\pi^{1/2} c A_n^{1/2}. \tag{30}$$

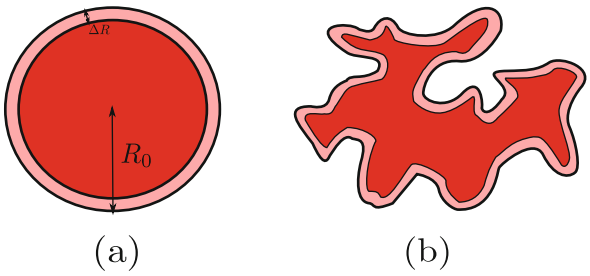

Fig. 10 Two tumors with a destroyed layer. (**a**) A tumor with the shape of a disk and initial radius R_0. At each step the immune system erases a layer (light red), reducing its radius by an amount ΔR. (**b**) Again a tumor with a destroyed layer, but exhibiting a more complex geometry (figure obtained from Ref. [45])

We assume that the superficial cell density σ of the tumor is approximately constant, which was missing in previous works. Finally, if the tumor is big enough so that the time intervals can be considered infinitesimal and defining a decay constant as $d = 2\pi^{1/2}\sigma^{1/2}c$, we obtain the differential equation

$$\dot{T} = -dT^{1/2}. \tag{31}$$

More simply, if we consider a disk of area $A = \pi R^2$ and assume that the velocity at which the radius decreases is constant $\dot{R} = -c$, with $c > 0$, we can write

$$\frac{dA}{dt} = 2\pi R\frac{dR}{dt} = -2\pi^{1/2}cA^{1/2}. \tag{32}$$

If the tumor has a more sophisticated geometry, we can still apply Eq. (31) under appropriate assumptions. Things get even more complicated if we take an initial tumor which is not a convex set, as the one depicted in Fig. 10b. Even in the case in which all the immune cells act synchronously and are equally effective, the topology of the tumor might change during the process of lysis, becoming disconnected. Assuming equal decay rates d and using Eq. (31), it is straightforward to verify that the total area of two tumors with the shape of a disk does not decay as a whole with the same velocity than that of a single tumor with such shape and equal total area. The two small tumors decay faster, because the ratio between the perimeter and the enclosed area is larger. Analytically, this is simply a consequence of the nonlinear nature of Eq. (31). Therefore, we designate the mean value of the variations of the radius of such sequence of disks as ΔR. Then, we write the variation of the radius as $\delta_n \Delta R$, where δ_n accounts for the deviations with respect to the mean value that must be bounded. The map is now $R_{n+1} = R_n - \delta_n \Delta R$ and the area goes as $A_{n+1} = A_n + \pi\delta_n^2\Delta R^2 - 2\pi^{1/2}\delta_n \Delta R A_n^{1/2}$. Making the same assumptions as in the previous case, the final result is

$$\dot{T} = -d(t)T^{1/2}, \tag{33}$$

where $d(t) = 2\pi^{1/2}\sigma^{1/2}c\delta(t)$, and $\delta(t)$ a function which takes into account the deviations from Eq. (31) due to the change in morphology and connectedness at each step. In the results we show that these deviations due to a complex morphology are small for the connected tumors here examined. Therefore, the *parabolic decay* represented in Eq. (31) works well at reproducing the decay of the tumors in the limit in which they are completely surrounded by immune cells, as long as they are not formed by disconnected pieces and their shape does not differ too much from a spherical shape. An explicit relation between $\delta(t)$ and the geometrical properties of the tumor can be derived. It is given by the expression

$$\delta(t) = \sqrt{\frac{L^2(t)}{4\pi A(t)}}, \tag{34}$$

where $L(t)$ is the length of the boundary of the tumor, while $A(t)$ is the total area occupied. If the value of $\delta(t)$ does not change substantially along the process of lysis, we can approximate the parameter as $d = 2\pi^{1/2}\sigma^{1/2}c\delta_0$.

5.2 *The Effects of Morphology on the Maximum Fractional Cell Kill*

We use the same cellular automaton model to inspect three different morphologies of two-dimensional tumors: a spherical tumor, a papillary tumor, and a filamentary tumor. The tumors generated with the cellular automaton are shown in Fig. 11. We place these three tumors inside a circumference and, for each of them, we repeat the experiments for several initial conditions. To this end, we fill with immune

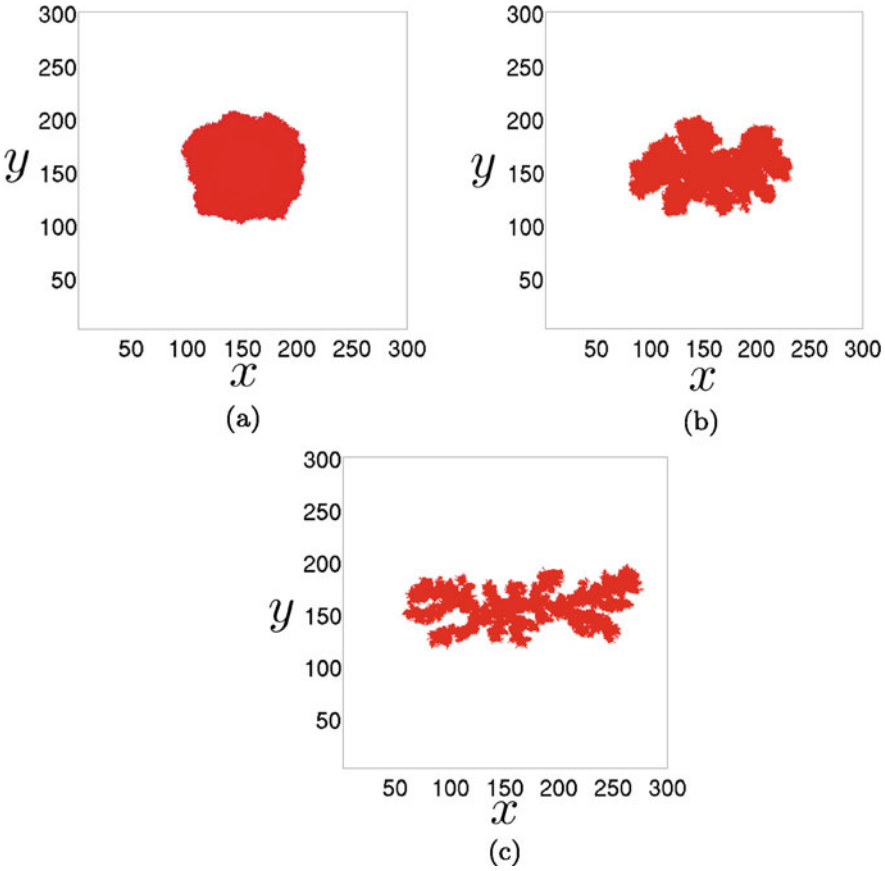

Fig. 11 Three tumors grown by iteration of the cellular automaton. A grid of $n \times n$ cells, with $n = 300$ has been used. We disregard necrosis and motility of tumor cells by setting the parameters, $\theta_{nec} = 0$ and $\theta_{mig} = \infty$. In all the three cases $\lambda_M = 10$. (**a**) A spherical tumor obtained for parameter values $\alpha = 2/n$, $\lambda_N = 25$, and $\theta_{div} = 0.3$. (**b**) A papillary tumor obtained for parameter values $\alpha = 4/n$, $\lambda_N = 200$, and $\theta_{div} = 0.3$. (**c**) A filamentary tumor obtained for parameter values $\alpha = 8/n$, $\lambda_N = 270$, and $\theta_{div} = 0.3$. These three tumors have grown up to approximately 9100 cells (figure obtained from Ref. [45])

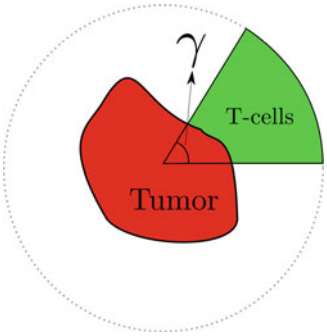

Fig. 12 How the initial conditions are set to investigate the lysis of the different tumors. The tumors are inscribed in a circumference and immune cells are placed in the surroundings for different angles γ. Since those cells that are not close to the tumor outer layer become inactivated during the first steps of the CA, small values of the angle correspond to the case shown in Fig. 8a, while the case $\gamma = 2\pi$ is related to Fig. 8c (figure obtained from Ref. [45])

cells the remaining space of the circumference for increasing angles, as depicted in Fig. 12. The time series representing the decay of the tumors are shown in Fig. 13. As explained in previous sections, we see a tendency towards linearity as the tumor is initially less covered with immune cells. Even the curvature is inverted for such small values of the initial angle, but this is surely a consequence of recruitment in the cellular automaton. Note also that the stochastic effects are more noticeable when the number of initial effector cells is low.

The cases in which the tumors are totally covered with immune cells as initial conditions ($\gamma = 2\pi$) are fitted to the equation $\dot{T} = -dT^{\nu}$ and also to $\dot{T} = -dT$, to elucidate which type of decay represents better the tumor cell lysis. The parameters are obtained through a least-square fitting method, and are listed in Table 5. As it can be seen in Fig. 14, the exponential decay is much worse at describing the time evolution of this dynamical system. Moreover, the value of ν that gives the best fit to the power-law function is equal to one half for the papillary and the filamentary tumors, and practically one half for the spherical case. The agreement is striking and, as previously predicted, the fluctuations are higher when the tumors exhibit a more complex geometry. Concerning the parameter d, we see that more branchy tumors display higher values. The explanation for this behavior is evident, since the higher it is the contact surface of a tumor, the more cells that can interact with it and the faster the speed at which it is lysed. This is in conformity with results obtained in the previous sections, where it was claimed that tumors with a spherical symmetry are harder to lyse. The crucial concept here is the accessibility that the immune cells have to the tumor cells.

Thus, we have demonstrated that in the limit in which a solid tumor is totally covered with immune cells, the velocity at which it decays is slower than exponential. This fact requires modifying Eq. (27) so that such limit is attained. The mathematical arguments previously employed can be perfectly extended to tumors

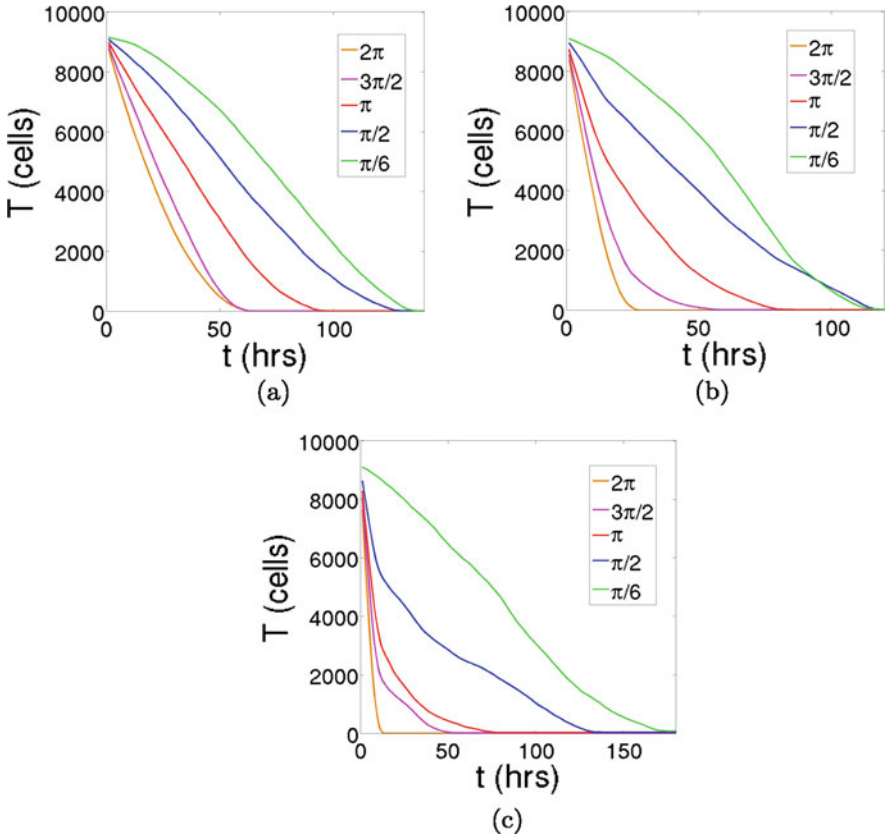

Fig. 13 The decay of the three tumors for different initial conditions. The immune cells are placed in the neighborhood of the tumors for values of the angles $\gamma = \{\pi/6, \pi/2, \pi, 3\pi/2, 2\pi\}$ and we iterate the CA. The CA actions corresponding to the lymphocytes have parameter values $\theta_{lys} = 0.3$, $\theta_{rec} = 0.5$, and $\theta_{inc} = 0.5$. The tumor cells dynamics has been frozen, and the parameters related to the diffusion of nutrients are the same as those appearing in previous figures. (**a**) The decay of the spherical tumor for the different initial conditions. (**b**) The decay of the papillary tumor for the different initial conditions. (**c**) The decay of the filamentary tumor for the different initial conditions. As less immune cells are placed in the vicinity of the tumors as initial conditions (from $\gamma = 2\pi$ to $\gamma = \pi/6$), the parabolic decay transforms into a more or less linear type of decay (figure obtained from Ref. [45])

that live in a three-dimensional space. If we recall that saturation of the velocity must be attained in the limit of infinitely big tumors, we propose that the kinetics of tumor lysis in the cell-mediated immune response to tumor growth is given by

$$\dot{T} = -d\frac{E^{\lambda}}{sT^{\nu} + E^{\lambda}}T^{\nu}, \tag{35}$$

Table 5 The parameter values of the power-law decay $\dot{T} = -dT^{\nu}$ and the exponential decay $\dot{T} = -dT$, to which the data of the cellular automaton are fitted by means of a least-squares fitting method

Power-law decay			Exponential decay		
Parameter	Units	Value	Units	Value	Description
d(s)	cell$^{1/2}$ h^{-1}	1.34	h^{-1}	0.04	Rate of decay
d(p)	cell$^{1/2}$ h^{-1}	3.36	h^{-1}	0.10	Rate of decay
d(f)	cell$^{1/2}$ h^{-1}	7.31	h^{-1}	0.21	Rate of decay
ν(s)		0.49			Exponent
ν(p)		0.50			Exponent
ν(f)		0.50			Exponent

We see that as the geometry of the tumor changes from spherical (s) through papillary (p) to filamentary (f), the parameter d increases. However, the value of ν is almost the same for the three geometries (table obtained from Ref. [45])

where the exponent ν depends on the dimension of the space, the morphology of the tumor and its connectedness. For realistic, connected, and rather spherical solid tumors we have $\nu = 2/3$, with the 2 standing for surface, and the 3 for volume. However, in those cases in which the tumor is very disconnected and the immune cells are well mixed with the tumor cells, as, for instance, in hematological cancers or solid tumors profusely infiltrated with lymphocytes, $\nu = 1$ should be used. The exponential decay arising in the limit $E_0^{\lambda} \gg sT$ would be then interpreted from a stochastic point of view, regarding the process as a Poisson process. Indeed, not all the immune cells have the same capacity to recognize a tumor cell, neither they act synchronously. In this case, the decay of a tumor does not differ substantially from other types of decay phenomena, as, for example, one-decay processes in radioactivity. For intermediate situations, the exponent ν will take a value between $2/3$ and 1.

6 Dynamics of Tumor–Immune Aggregates

To conclude this study we use a hybrid cellular automaton to investigate the dormancy of a tumor mass, mediated by the cellular immune response. Even though an interesting work has been previously carried out in this context [40], the present study includes new features, which we believe makes it more realistic, permitting a correlation between the results and the theory of immunoedition. Mainly, the time scale of the cytotoxic cell action (about 1 h) differs from the time scale of tumor cell proliferation (about 1 day). Secondly, our cellular automaton includes a new parameter that allows us to represent immunosuppressed environments.

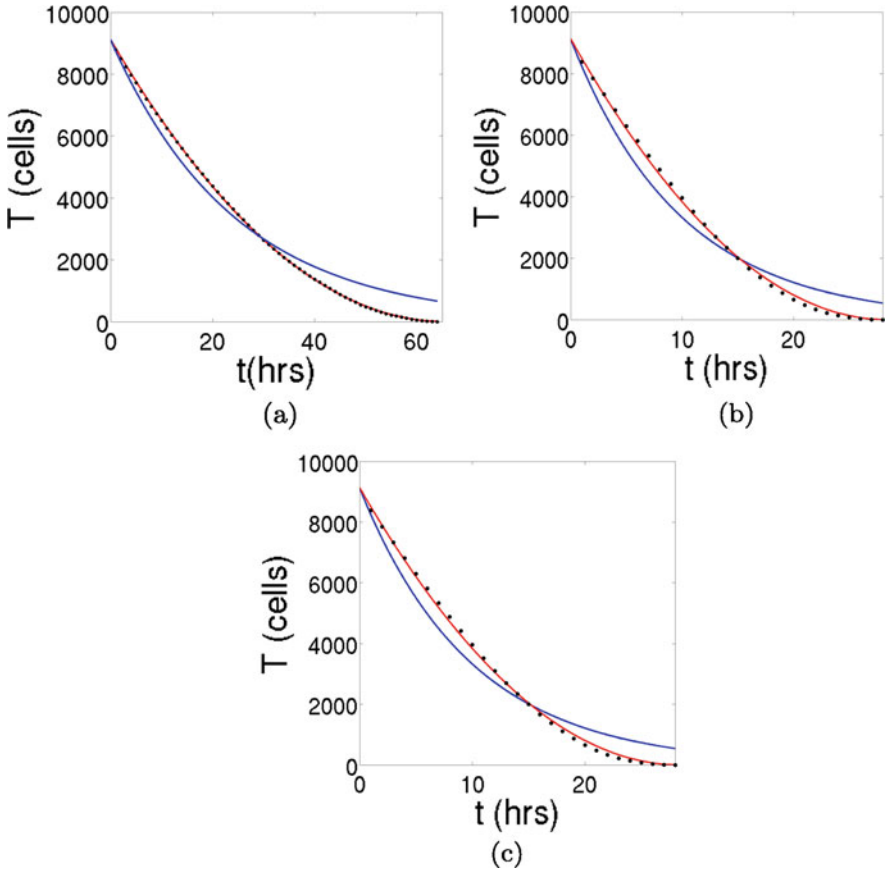

Fig. 14 The decay of the three tumors for $\gamma = 2\pi$. We have iterated the cellular automaton in the limit in which the tumors are totally covered with immune cells. The results are fitted to a power-law function $\dot{T} = -dT^{\nu}$, shown in red, and an exponential decay $\dot{T} = -dT$, shown in blue, to elucidate which type of decay represents better the velocity with which the tumors shrink. (**a**) The decay of the spherical tumor. (**b**) The decay of the papillary tumor. (**c**) The decay of the filamentary tumor. In all the cases a power-law function with an approximate value of $\nu = 1/2$ fits much better the results of the CA. Therefore, the decay is parabolic. The exact values are listed in Table 5 (figure obtained from Ref. [45])

The exploration of different immunological scenarios enables the discussion of a possible dynamical origin of tumor dormancy and the sneaking through of tumors, as originally proposed by Kuznetsov et al. [31]. Before embarking on this study, some information on the immunoediting of tumors is deserved.

6.1 Cancer Immunoedition

Cancer immunoediting can be described by three phases: elimination, equilibrium, and escape. The first of these three Es [52] corresponds to what has traditionally been termed immunosurveillance [53], and involves the innate and the adaptive immune responses. During this phase, the immune system keeps in check a tumor cell population, successfully recognizing and destroying the majority of its cells. However, some residual tumor cells might remain unnoticed and asymptomatic for a long period of time, which can range from 5 years to more than 20 years. This period of time defines a second stage, in which a small cell population is kept at equilibrium. Finally, the phase of escape is led by some tumor cells that might present a priori or have acquired along their evolutionary process, a non-immunogenic phenotype.

The mechanisms through which a tumor can be maintained at low cell numbers (i.e., dormant) are diverse. In a first approach, cancer dormancy can be generally classified into two categories: tumor mass dormancy and cellular dormancy [54]. In the former case, the equilibrium of a tumor is the result of a balance between cell growth and cell death. In the latter, the cells arrest and survive in a quiescent state until more benevolent conditions are provided by their environment. The occurrence of tumor mass dormancy is commonly associated with two different mechanisms [55]. The first is angiogenic dormancy, which occurs when the cells are unable to induce angiogenesis, and therefore to recruit oxygen and other nutrients to their location. In this manner, the proliferation rate is counterweighted by elevated rates of apoptosis. The second mechanism is the immune system response. This response is very complex and involves many types of cells and molecules [43]. There is evidence that the cell-mediated immune response collaborates with the humoral immune response to promote the dormancy of tumors, and that $CD8^+$ lymphocytes and IFN-γ play a transcendental function in its maintenance [56].

6.2 Cellular Automata Rules Revisited

Most of the CA rules for the tumor and the cytotoxic cells are the same as before. However, one more action concerning the immune cells is included and the algorithm is modified to allow for the coevolution of both cell populations. Such an action corresponds to a constant input of cytotoxic cells into the domain (Fig. 15). Even though we do not make a distinction between the innate and the adaptive immune responses, this constant source of immune cells allows to model the presence of NK cells in a tacit manner. These cells are placed at random in the domain, at points that are not occupied by tumor cells. Every such grid point is examined and, if a probabilistic condition holds, the healthy or dead cells that might occupy it are replaced with an immune cell. An immune cell is placed in the background with probability

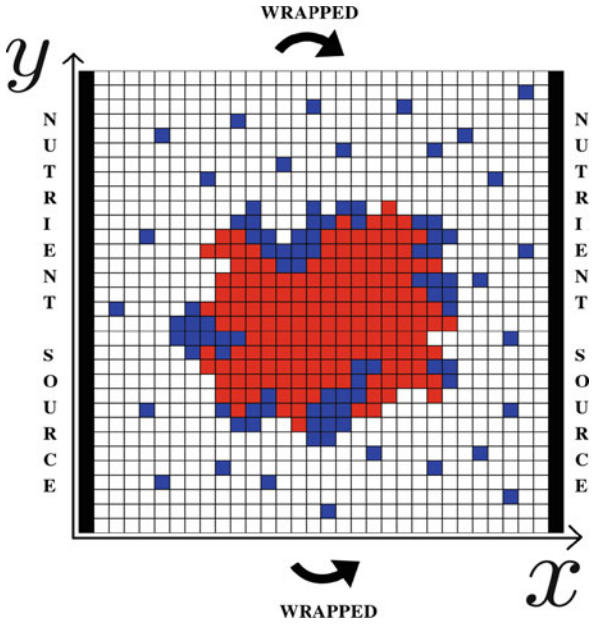

Fig. 15 The cellular automaton. A grid representing the cellular automaton during the growth of a tumor in the presence of immune effector cells. The tumor cells are shown in red and the immune cells appear in blue. The remaining spots are occupied by healthy or dead cells. The vertical black stripes in the boundary of the square domain represent the vessels from which nutrients diffuse. Periodic boundary conditions are considered in the remaining part of the boundary. Some immune cells are scattered in the region, and some other form clusters that advance reducing the tumor (figure obtained from Ref. [47])

$$P_{bkg} = f - \frac{1}{n^2} \sum_{i \in \mathrm{CA}} E_i, \tag{36}$$

where f is a number between 0 and 1 that represents the intensity of the input of immune cells into the tissue. If P_{bkg} is greater than a randomly generated number between zero and one, then an immune cell appears in the corresponding grid point.

Again, the algorithm starts with a domain full of healthy cells, except for a single tumor cell placed at the center of the domain. Firstly, we let the tumor grow until it is detected by the immune system, when it has reached some specific size T_{det}. During this period of growth, each CA step corresponds to 1 day. Each iteration begins with the integration of the reaction–diffusion equations, using a finite-difference scheme and a successive overrelaxation method. Then all the tumor cells are randomly selected with equal probability, and the CA rules are applied. As in previous works [41], every time an action takes place, the reaction–diffusion equations are locally solved in a neighborhood with size 20×20 grid points. When the time of detection is reached, the immune cells start to evolve. Now the CA step corresponds to 1 h, and during the next twenty-three steps, only the immune cells are computed. First, the background source of immune cells is executed. Then, the reaction–diffusion equations are solved and all the immune cells are randomly selected. For each immune cell, after applying the CA rules, the nutrients are computed in a local region, in exactly the same manner as before. Every twenty-three iterations, the tumor cells are checked and the tumor cell rules are applied as previously described, before immune detection. The algorithm stops when a maximum number of steps

after the elapse of the immune response have been reached or when a tumor cell is at a distance of two grid points from its boundary.

6.3 Simulations and Results

We study the evolution of the tumor and the immune system for three different scenarios. The first scenario is used as a reference, and it is characterized by high levels of immune cell recruitment and negligible necrosis due to the scarcity of nutrients in the core of the tumor masses. In the second scenario, the recruitment levels are reduced, while the necrosis of tumor cells is enhanced in the third. Unless specified, the remaining parameters are all the same in every case. Beginning with one tumor cell, the tumors grow up to $T_{det} = 5 \times 10^3$ cells, and at this moment the immune response triggers. In order to elucidate the effects of tumor immunogenicity, we devise what shall be called a *transient bifurcation diagram*. Given a dynamical system, a bifurcation diagram is a plot of the asymptotic values of a particular variable against a set of values of some relevant parameter. However, in many situations there might exist very long transients before the asymptotic state is established. These transients are of great importance in our context, since tumors may exhibit long periods of latency before the development of recurrence. Therefore, we compute the number of tumor cells for the last 100 iterations of a trajectory comprising 24,000 iterations of the CA from immune detection. Then, these 100 points are represented on the vertical axis for different values of the parameter θ_{lys}, which lies on the horizontal axis. If we assign to each of these iterations a time of 1 h, we are registering the size of the tumor for approximately the last 4 days of a period of 33 months from immune detection. We recall that the parameter θ_{lys} codes the intrinsic ability of the immune cells to recognize and lyse their adversaries. Higher values of this parameter correspond to more immunodeficient environments.

6.3.1 Reference Scenario

The set of parameters for this scenario is chosen similar to previous works, in which it has been demonstrated that they generate reasonable tumor dynamics [41, 46]. The specific values are $\theta_{div} = 0.3$, $\theta_{nec} = 0.05$, $\theta_{mig} = \infty$, $\theta_{rec} = 1.0$, $\theta_{inc} = 0.1$, $\lambda_M = 10$, $\lambda_N = 25$, and $\alpha = 2/n$. Regarding the natural flow of immune cells into the tissue, two situations are inspected for each scenario. The first corresponds to a high input of immune cells into the tumor area. In this case a value $f = 0.10$ is set, which means that approximately 10% of the background is occupied by immune cells, if there are not too many immune cells piled up. The other has a lower input of 5%, thus $f = 0.05$. In the absence of immune response, the tumors display a rather spherical shape. As we can see from the transition bifurcation diagrams shown in Fig. 16, three different regions are clearly distinguished. In the first region, when

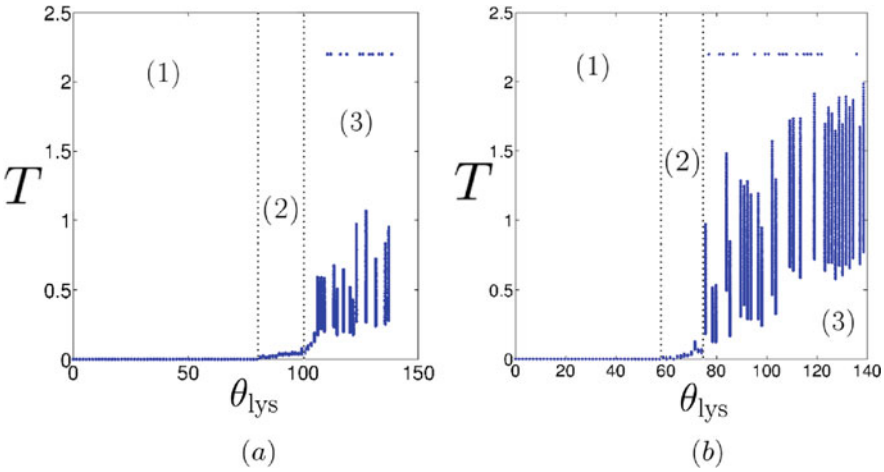

Fig. 16 Transient bifurcation diagrams. Two transient bifurcation diagrams for the reference scenario. The size of the tumor T for the last 100 h of a trajectory comprising 1000 days is plotted against the parameter that models the immunogenicity of the tumor θ_{lys}. The size of the tumor has been "normalized," dividing it by the number of total grid points n^2. Tumors having escaped the region are assigned a value of $T = 2.2$, which is over the maximum obtained in all our simulations. (**a**) A transient bifurcation diagram for a constant input of tumor cells into the domain given by $f = 0.1$. (**b**) A transient bifurcation diagram for a constant input of tumor cells into the domain given by $f = 0.05$. Three different regimes are clearly discerned. The first (1) corresponds to the elimination of the tumors, the second (2) to abiding small tumors kept in equilibrium by the immune cells, and the third (3) to fast growing tumors that escape the domain (figure obtained from Ref. [47])

the immune system is effective, the tumors are completely eliminated. The second is related to an equilibrium phase, for which tumors spend very long transients oscillating at low cell numbers. Finally, tumors with increasing size, eventually leaving the domain through the vessels, appear in the third region. Thus, here we see how immunogenicity affects the fate of tumors, in accordance with the theory of immunoedition.

To give insight into the second and the third regions, time series have been computed (see Figs. 17 and 18), until the tumor escapes. Initially, the tumors grow in the absence of immune response, and then the immune cells start to reduce them or, in the worst case, delay their growth. Depending on how effective the immune cells are, longer or shorter transients follow this reduction phase. The asymptotic dynamics is always the same: if the tumors are not totally eliminated by an efficient immune system, they eventually escape from the region. These two attractors are reminiscent of those appearing in reference [31]. As shown in Fig. 17a, the length of the transients in the second region, which are of around 12 years, clearly indicate a phase of prolonged tumor mass dormancy. During the period of dormancy the immune system keeps the tumor at low cell numbers and randomly displaces its disconnected pieces until one of them reaches the vessels. In the third region,

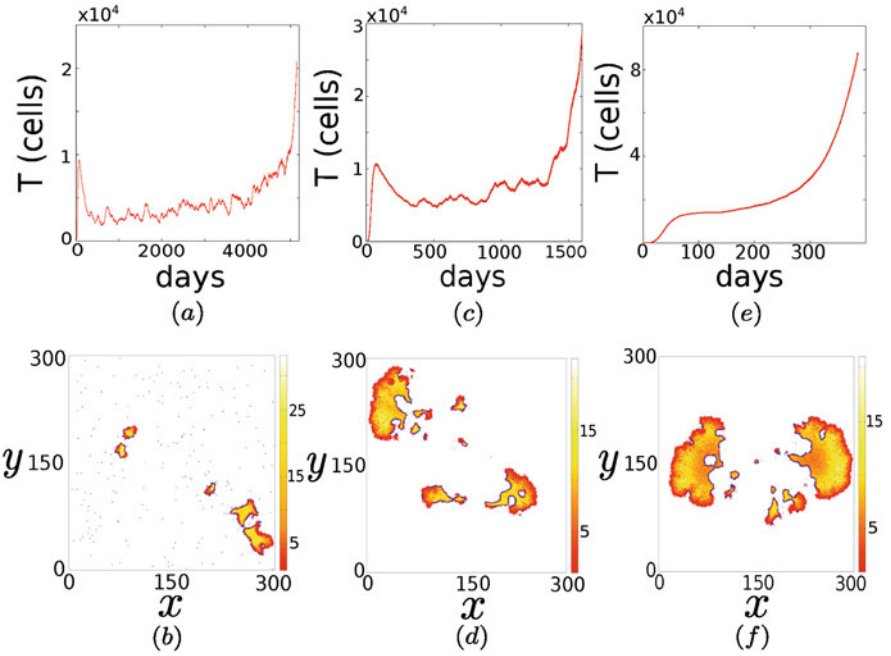

Fig. 17 Asymptotic dynamics and tumor escape. Three time series of the tumor size for the reference scenario are plotted. The constant input of immune cells to the domain is $f = 0.1$. The size of the tumors is registered until they escape the domain through the vessels. The corresponding tumors at escape are shown below. The color bar represents the number of tumor cells at a grid point. For clearness, the immune cells at a grid point are simply colored in dark blue. The dead cells are represented in light blue. (**a**) A long-lived tumor is kept at equilibrium for $\theta_{lys} = 90$. This is an example of immune-mediated tumor mass dormancy. (**b**) The corresponding small tumor at escape. (**c**) A less immunogenic tumor $\theta_{lys} = 106$ is kept at equilibrium, but for a considerably shorter time. (**d**) The corresponding tumor at escape, which is noticeably bigger compared to the previous case. (**e**) A tumor that is barely immunogenic for $\theta_{lys} = 140$. Now the tumor escapes very rapidly and exhibits the largest size, although the immune system delays its growth. (**f**) The corresponding tumor at escape (figure obtained from Ref. [47])

transients are found again, but they are shorter (less than 4 years) and the tumors at escape have bigger sizes. As predicted by Kuznetsov et al. [31], the duration of the transients is stochastic. This randomness is evident from the transient bifurcation diagrams, since after 33 months of tumor–immune struggle, some tumors have escaped and some others have not, disregarding how immunogenic they are. When the immune system barely responds to the tumor, we see very big tumors occupying the domain and escaping rapidly, as depicted in Fig. 17e.

Interestingly, the equilibrium region shrinks as the normal input of cells into the tissue reduces from $f = 0.1$ to $f = 0.05$. As it is shown in Fig. 18, the oscillations during the equilibrium phase are more pronounced. This makes the equilibrium more unstable and suggests that having cells scattered all over the

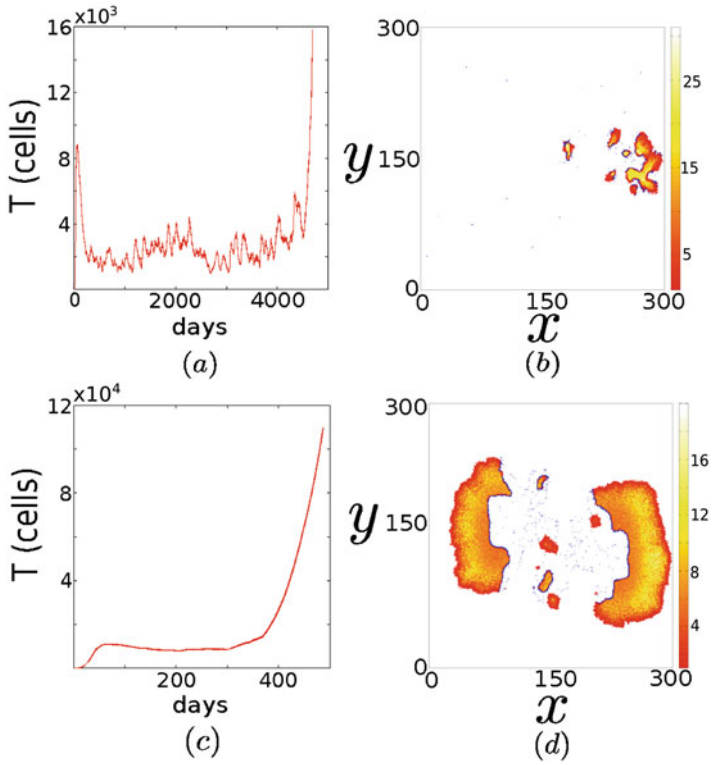

Fig. 18 Asymptotic dynamics and tumor escape. Two time series of the tumor size and the corresponding tumors at escape are plotted for the reference scenario. The constant input of immune cells to the domain is now smaller $f = 0.05$. (**a**) A long-lived tumor is kept at equilibrium for $\theta_{lys} = 67$. Now the oscillations of the tumor size during the equilibrium are higher. (**b**) The corresponding tumor at escape, which again is small. (**c**) Another tumor $\theta_{lys} = 89$ that is slightly reduced and kept at a constant size for a year, but that soon after escapes. (**d**) The corresponding tumor at escape (figure obtained from Ref. [47])

domain is important for the maintenance of dormancy. Probably, the reason is that these spread immune cells keep the tumor at a small size, not allowing its overgrowth in any specific direction.

We have also explored the importance of the tumor size at detection by reducing this size to 5×10^2 cells. The results are depicted in Fig. 19 and resemble very much those shown in Fig. 16. There is no hint of a sneaking through mechanism in our model. According to the definition given by Gatenby et al. [57], sneaking through is the preferential take of tumors after small size inocula to a similar degree with that seen with large size inocula, compared to the rejection of medium sized inocula. More clearly put, small and big tumors escape immune surveillance, while intermediate do not. Such phenomenon has not been observed in the present case for other values of the tumor size at detection. However, we do not discard it, since

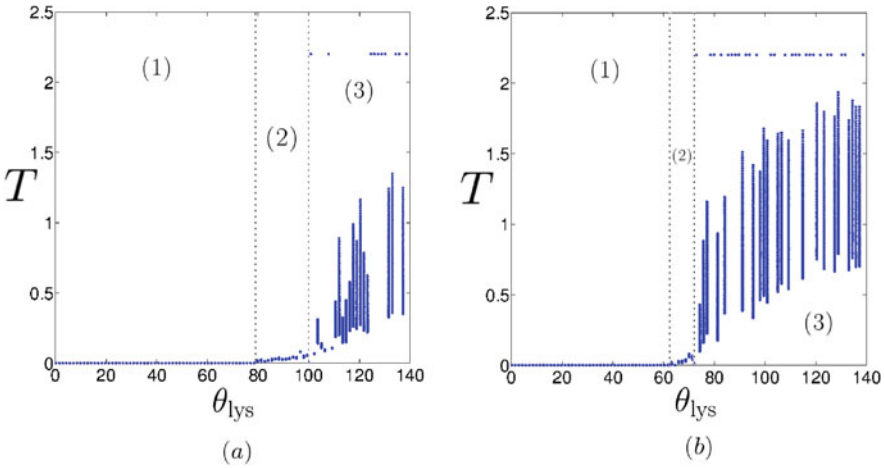

Fig. 19 Transient bifurcation diagrams. Two transient bifurcation diagrams for the reference scenario. Now a smaller tumor size at detection $T_{det} = 500$ has been considered. (**a**) A transient bifurcation diagram for a constant input of tumor cells into the domain given by $f = 0.1$. (**b**) A transient bifurcation diagram for a constant input of tumor cells into the domain given by $f = 0.05$. The effects of tumor size at detection does not introduce significant changes in the dynamics (figure obtained from Ref. [47])

motility of tumor cells has not been included in this first investigation, and might be crucial for these cells to escape.

Finally, even though the tumors here inspected are genetically homogeneous and no evolutionary process is really taking place in our model, the transient bifurcation diagrams insinuate how the sculpting of the phenotype occurs, moving from the first region to the second, and then to the third. In fact, a similar cellular automaton can be used to explore the impact of heterogeneity and how the process of immunoedition takes place. It suffices to consider that the immune cells intrinsic cytotoxicity, represented by the parameter θ_{lys}, depends on the tumor cell.

6.3.2 Low Recruitment Scenario

We now evaluate the impact of the recruitment of immune cells to the domain of the tumor. For this purpose, we reduce the value of θ_{rec} from 1 to 0.35. Our interest in this parameter is due to the fact that, in many occasions, the recruitment of cells to the site of the tumor might be very complicated. The recruitment of immune cells is a very complex process, at least from a physical point of view. The extravasation of leukocytes requires an initial contact between these cells and the endothelial cells, which depends on adhesion molecules. After adhesion to the walls of the vessels, the immune cells traverse them through diapedesis, which again relies on several cytokines. Finally, chemokines bias their random walks to the tumor location [58].

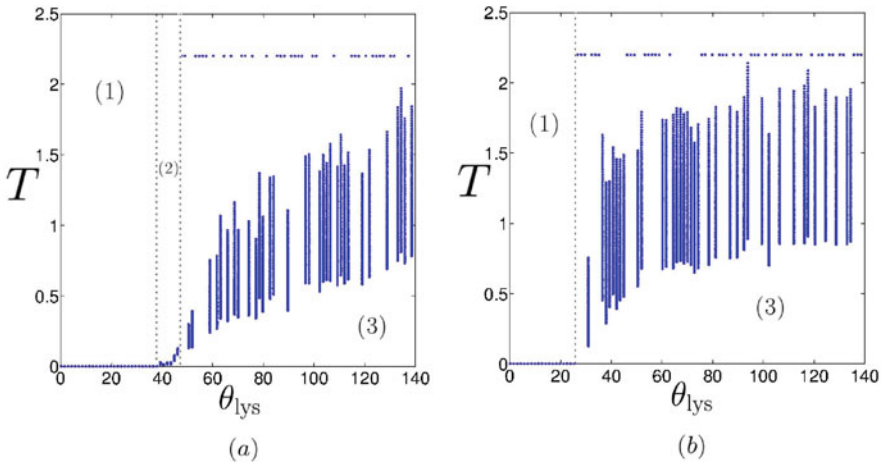

Fig. 20 Transient bifurcation diagrams. Two transient bifurcation diagrams for the low recruitment scenario $\theta_{rec} = 0.35$. (**a**) A transient bifurcation diagram for a constant input of tumor cells into the domain given by $f = 0.1$. (**b**) A transient bifurcation diagram for a constant input of tumor cells into the domain given by $f = 0.05$. A decrease of the immune cell recruitment value reduces the window of equilibrium. Thus large periods of dormancy require significant levels of immune cell recruitment (figure obtained from Ref. [47])

Thus we expect this parameter to exhibit great fluctuations, depending on the tissue location and other factors, as, for instance, the degree of inflammation.

The effects of decreasing the recruitment parameter are shown in Fig. 20. As expected, the elimination region shrinks, while the escape region widens. A dramatic reduction of the dormancy window is observed in both plots. When $f = 0.1$, the window still exists, but for $f = 0.05$ it has even disappeared. These results suggest that a relatively tight balance between lysis and growth is required to maintain the dynamical equilibrium of the tumor.

Note that, as previously proposed, the equilibrium of the tumor implies that reduction must occur in an isotropic manner. If a region of the tumor grows over the immune system capacity, then a soon overgrowth and a consequent escape would be expected. In the present model, this relies on a positive feedback mechanism between the natural input of immune cells and their recruitment. The more cells there are spread in the domain, the more chances for an immune cell to lethally hit a tumor cell. When this occurs, recruitment proceeds, favoring the local aggregation of immune cells at this site of the tumor and giving rise to satellites [40]. This isotropy can be appreciated in the equilibrium represented in Figs. 17b and 18b, as opposed to those situations that lie in the third region, represented in Figs. 17d, f and 18d.

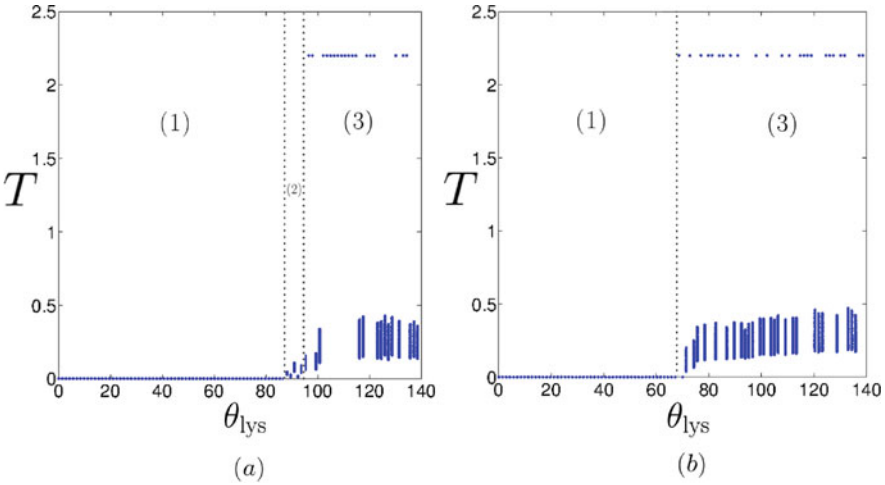

Fig. 21 Transient bifurcation diagrams. Two transient bifurcation diagrams for the high necrosis scenario $\theta_{nec} = 1.0$. (**a**) A transient bifurcation diagram for a constant input of tumor cells into the domain given by $f = 0.1$. (**b**) A transient bifurcation diagram for a constant input of tumor cells into the domain given by $f = 0.05$. The window of equilibrium has been reduced again, which suggests that long-lived periods of dormancy are based on a delicate equilibrium between the proliferation rate of the tumor and its lysis by the immune system (figure obtained from Ref. [47])

6.3.3 High Necrosis Scenario

Solid tumors exhibit sometimes necrotic cores due to the scarcity of nutrients. Other chemical species can be represented with the present model (e.g., growth factors) and, if desired, necrosis can be regarded as apoptosis, at least to some extent. Therefore, we now inspect the effects of cell death in the model. To this end, we increase the value of θ_{nec} from almost zero to 0.5. Obviously, the increase of necrosis facilitates the labor of the immune system. As shown in Fig. 21, the elimination region enlarges substantially, compared to the reference case. Also in the equilibrium region, lower tumor cell numbers are seen before the escape of the tumor. More importantly, the equilibrium window, which has been associated with large periods of tumor mass latency, is practically imperceptible for $f = 1.0$ and has completely vanished for $f = 0.05$. We have again computed time series, showing that transients occur in the equilibrium region, sometimes as long as those appearing before in the equilibrium, but generally shorter (see Fig. 22). In fact, the equilibrium window and the escape zone drawn in Fig. 21a overlap. It seems that the equilibrium region appearing in the reference scenario has been swept under the elimination region. Once more, the results confirm the requisite of a relatively delicate balance between the mechanisms that maintain the cytotoxic destruction of the immune system and the growth of the tumor, in order to keep it at low cell numbers for long periods of time.

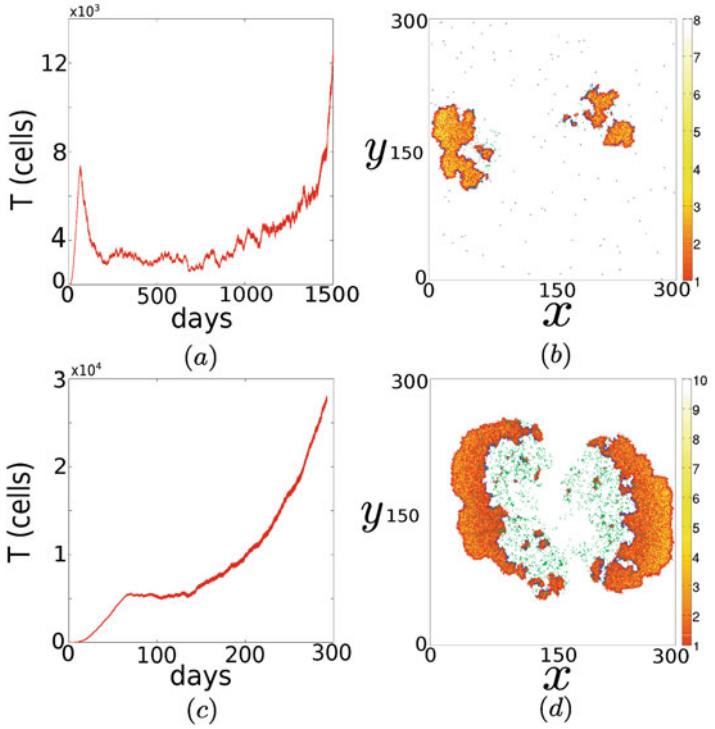

Fig. 22 Asymptotic dynamics and tumor escape. Two time series of the tumor size for the reference scenario are plotted. The constant input of immune cells to the domain is now smaller $f = 0.05$. The size of the tumors is registered until they escape the domain. The tumors at escape are shown beside. Again, the immune cells appear in dark blue, while the tumor cells range from red to white. The dead cells, which also appear inside the tumor, are now represented in green. (**a**) A quite long-lived tumor is kept at equilibrium for $\theta_{lys} = 92$. (**b**) The corresponding tumor at escape. (**c**) Another tumor $\theta_{lys} = 118$ that is barely reduced and kept at a constant size for less than half a year, and then escapes rapidly. (**d**) The corresponding tumor at escape (figure obtained from Ref. [47])

7 Conclusions

In the present chapter we have explored the dynamics of tumor growth in the presence of an immunological response. This formidable task would have been much more difficult without the aid of cellular automata, which are discrete spatio-temporal models that allow to represent complex biological systems. The main idea is to use this sophisticated modelling framework to perform in silico experiments, which allow to reproduce the tissue environment as an open system. Of course, and just as it occurs with in vitro experiments, the design of these models relies upon several hypotheses, which must be thoroughly debated.

Using a hybrid cellular automaton, we have shown that cell crowding is a plausible candidate that can explain the saturation of the fractional cell kill of tumor cells by their cytotoxic opponents observed in immunological assays on the lysis of tumors. This limitation depends on the morphology of the tumor, insofar as geometry restricts the access of effector cells to tumor cells. In theory, those tumors growing with “spherical symmetry" will be the harder to lyse, because more layers of tumor cells have to be erased to reach the cells at the center. Nevertheless, we recall that the process of T cell recruitment from circulation to the tumor site is complex, involving several steps [59]. This implies that the crowding might happen before contact with the tumor occurs, as, for example, during adhesion to the endothelium. In such a case, a relation between the parameters in the fractional cell kill and the shape of the tumor cannot be established. Furthermore, we have explored the decay laws that govern the destruction of the tumor for the extreme situations in which the immune response is too weak or very strong. We have observed that, when there is no infiltration, the decay ranges from a linear decay to a parabolic decay. The linear decay corresponds to small values of the effector-to-target ratio as initial conditions, while the parabolic decay represents a tumor that is widely surrounded by immune cells. Intermediate situations are governed by Eq. (35).

The significance of this new mathematical function can be described as follows. The rate at which a tumor as a whole is destroyed by a population of immune cells increases as the both cell populations increase. However, at some point, saturation is attained. The particular functional response is given by a Hill function depending on both cell populations, in a quite symmetrical way. In the case of the effector cells, this extrinsic barrier to the lytic capacity is reflected in the parameters d and λ. These parameters depend on the geometry of the tumor. Less spherical tumors correspond to higher values of both parameters. Interestingly, the values of λ are expected to be between zero and one, as suggested by the experiments and the simulations. From the enzymatic kinetics point of view, this can be interpreted as non-cooperative binding. Certainly, if we pay attention to the process of lysis only, the best that an immune cell can do to another is not to interpose between itself and their adversaries. Of course, cooperative effects exist, as the recruitment term exemplifies. Quite the opposite, as the intrinsic lytic capacity of cytotoxic cells is decreased, saturation gradually vanishes. This capability is inversely proportional to the parameter s. On the other hand, the saturation of the lytic velocity due to a tumor of increasing size is reflected in the parameters ν, which depends on the degree of infiltration or, if desired, on its topology. More connected tumors have smaller values of this parameter, ranging from one to two-thirds (in the case of three-dimensional tumors).

Finally, we have studied the transient and asymptotic dynamics of a cellular automaton model for tumor–immune interactions. We have shown that, depending on the immunogenicity of the tumor, the model furnishes three main types of dynamics, which are in close relationship with the three phases of the theory of immunoedition. Importantly, we have shown that a dynamical equilibrium between the tumor can occur for long periods of time, as proposed by Kuznetsov et al. [31]. However, after inspection of the parameter space, our model suggests that

this equilibrium is quite fragile, since it is based on an adjusted balance between the mechanisms that stimulate the immune response and tumor cell proliferation. This also occurs in the model presented by these authors [31], since considerable levels of recruitment are required to sustain dormancy. Furthermore, the infiltration of the immune cells into the tumor mass has been neglected in the present work. We also recall that the piling of immune cells in this study has been restricted, to speed the extensive computations. Presumably, these effects would make the equilibrium much more delicate. Nevertheless, both models clearly demonstrate that a state of tumor mass dormancy mediated by the immune system is possible. It is the length of this dormant period that can be safely questioned. Thus, we conclude that, even though tumor mass dormancy can result from the cell-mediated immune response to tumor growth, long periods of dormancy, as commonly found in recurrent metastatic tumors [54, 55], are not likely to arise by this single mechanism. It is therefore pertinent to ask ourselves if the role of the cell-mediated immune response in the promotion of the dormancy of a tumor mass is rather to synergize with other types of more efficient mechanisms, as, for example, cellular dormancy.

Acknowledgements This work has been supported by the Spanish Ministry of Economy and Competitiveness under Project No. FIS2013-40653-P and by the Spanish State Research Agency (AEI) and the European Regional Development Fund (FEDER) under Project No. FIS2016-76883-P. M.A.F.S. acknowledges the jointly sponsored financial support by the Fulbright Program and the Spanish Ministry of Education (Program No. FMECD-ST-2016).

References

1. D. Hanahan, R.A. Weinberg, Hallmarks of cancer. Cell **100**, 57–70 (2000)
2. D. Hanahan, R.A. Weinberg, Hallmarks of cancer: the next generation. Cell **144**, 646–673 (2011)
3. C. Sonneschein, A.M. Soto, The dead of the cancer cell. Cancer Res. **71**, 4334–4337 (2011)
4. C. Sonneschein, A.M. Soto, The aging of the 2000 and 2011 hallmarks of cancer reviews: a critique. J. Biosci. **38**, 651–666 (2013)
5. I.P. Witz, O. Levy-Nissenbaum, The tumor microenvironment in the post-PAGET era. Cancer Lett. **242**, 1–10 (2006)
6. P. Ehrlich, Über den jetzigen Stand der Karzinomforschung. Nederlands Tijdschrift voor Geneeskunde **5**, 273–290 (1909)
7. M.F. Burnet, Cancer-a biological approach: I. The processes of control. II. The significance of somatic mutation. Br. Med. J. **1**, 779–786 (1957)
8. M.F. Burnet, Immunological surveillance in neoplasia. Transplant. Rev. **7**, 3–25 (1971)
9. L. Thomas, in *Cellular and Humoral Aspects of the Hypersensitive State*, ed. by H.S. Lawrence (Hoeber-Harper, New York, 1959), pp. 529–533
10. O. Stutman, Tumor development after 3-methylcholantrene in immunologically deficient athymic-nude mice. Science **183**, 534–536 (1974)
11. O. Stutman, Immunodepression and malignancy. Adv. Cancer Res. **22**, 261–422 (1975)
12. D.H. Kaplan, V. Shankaran, A.S. Dighe, E. Stockert, M. Aguet, L.J. Old, R.D. Schreiber, Demonstration of an interferon γ-dependent tumor surveillance system in immunocompetent mice. Proc. Natl. Acad. Sci. U. S. A. **95**, 7556–7561 (1998)

13. V. Shankaran, H. Ikeda, A.T. Bruce, J.M. White, P.E. Swanson, L.J. Old, R.D. Schreiber, IFNγ and lymphocytes prevent primary tumor development and shape tumor immunogenicity. Nature **410**, 1107–1111 (2001)
14. L. Gattinoni, D.J. Powell Jr., S.A. Rosenberg, N.P. Restifo, Adoptive immunotherapy for cancer: building on success. Nat. Rev. Immunol. **6**, 383–393 (2006)
15. M. Kalos, B.L. Levine, D.L. Porter, S. Katz, S.A. Grupp, A. Bagg, C.H. June, T cells with chimeric antigen receptors have potent antitumor effects and can establish memory in patients with advanced leukemia. Sci. Transl. Med. **3**, 95ra73 (2011)
16. A. Ribas, L.H. Camacho, G. Lopez-Berestein, D. Pavlov, C.A. Bulanhagui, R. Millham, B. Comin-Anduix, J.M. Reuben, E. Seja, C.A. Parker, A. Sharma, J.A. Glaspy, J. Gomez-Navarro, Antitumor activity in melanoma and anti-self responses in a phase I trial with the anti-cytotoxic T lymphocyte-associated antigen 4 monoclonal antibody CP-675,206. J. Clin. Oncol. **23**, 8968–8977 (2005)
17. E.J. Lipson, W.H. Sharfman, C.G. Drake, I. Wollner, J.M. Taube, R.A. Anders, H. Xu, S. Yao, A. Pons, L. Chen, D.M. Pardoll, J.R. Brahmer, S.L. Topalian, Durable cancer regression off-treatment and effective re-induction therapy with an anti-PD-1 antibody. Clin. Cancer Res. **19**, 462–468 (2013)
18. P. Sharma, K. Wagner, J.D. Wolchok, J.P. Allison, Novel cancer immunotherapy agents with survival benefit: recent successes and next steps. Nat. Rev. Cancer **11**, 805–812 (2011)
19. L.A. Emens , L.H. Butterfield, F.S. Hodi Jr., F.M. Marincola, H.L. Kaufman, Cancer immunotherapy trials: leading a paradigm shift in drug development. J. Immunother. Cancer **4**, 42 (2016)
20. A.R. Anderson, A hybrid mathematical model of solid tumor invasion: the importance of cell adhesion. Math. Med. Biol. **22**, 163–186 (2005)
21. D. Basanta, A.R. Anderson, Homeostasis back and forth: an ecoevolutionary perspective of cancer. Cold Spring Harb. Perspect. Med. **7**, a028332 (2017)
22. P. Gerlee, A.R. Anderson, A hybrid cellular automaton model of clonal evolution in cancer: the emergence of the glycolytic phenotype. J. Theor. Biol. **250**, 705–722 (2008)
23. T. Alarcón, H.M. Byrne, P.K. Maini, A cellular automaton model for tumor growth in inhomogeneous environment. J. Theor. Biol. **227**, 257–274 (2003)
24. H. Enderling, L. Hlatky, P. Hahnfeldt, Migration rules: tumors are conglomerates of self-metastases. Br. J. Cancer **100**, 1917–1925 (2009)
25. J.N. Kather, J. Poleszczuk, M. Suarez-Carmona, J. Krisam, P. Charoentong, N.A. Valous, C. Weis, L. Tavernar, F. Leiss, E. Herpel, F. Klupp, A. Ulrich, M. Schneider, A. Marx, D.J. Jager, N. Halama, In silico modeling of immunotherapy and stroma-targeting therapies in human colorectal cancer. Cancer Res. **77**, 6442–6451 (2017)
26. N. Bellomo, L. Preziosi, Modelling and mathematical problems related to tumor evolution and its interaction with the immune system. Math. Comput. Model. **32**, 413–452 (2000)
27. L. Michaelis, M.L. Menten, Die Kinetik der Invertinwirkun. Biochem. Z. **49**, 333–369 (1913)
28. K.A. Johnson, R.S. Goody, The original Michaelis constant: translation of the 1913 Michaelis-Menten paper. Biochemistry **50**, 8264–8269 (2011)
29. J. Monod, The growth of bacterial cultures. Annu. Rev. Microbiol. **3**, 371–393 (1949)
30. C.S. Holling, Some characteristics of simple types of predation and parasitism. Can. Entomol. **91**, 385–398 (1959)
31. V.A. Kuznetsov, I.A. Makalkin, M.A. Taylor, A.S. Perelson, Nonlinear dynamics of immunogenic tumors: parameter estimation and global bifurcation analysis. Bull. Math. Biol. **56**, 295–321 (1994)
32. A.J. Lotka, Analytical note on certain rhythmic relations in organic systems. Proc. Natl. Acad Sci. U. S. A. **6**, 410–415 (1920)
33. V. Volterra, Variazioni e fluttuazioni del numero d´ individui in specie animali conviventi. Mem. Acad. Lincei Roma **2**, 31–113 (1926)
34. L.G. De Pillis, A. Radunskaya, The dynamics of an optimally controlled tumor model: a case study. Math. Comput. Model. **37**, 1221–1244 (2003)

35. A.G. López, J.M. Seoane, M.A.F. Sanjuán, A validated mathematical model of tumor growth including tumor-host interaction, cell-mediated immune response and chemotherapy. Bull. Math. Biol. **76**, 2884–2906 (2014)
36. A. Diefenbach, E.R. Jensen, A.M. Jamieson, D.G. Rauelt, Rae1 and H60 ligands of the NKG2D receptor stimulate tumor immunity. Nature **413**, 165–171 (2001)
37. M.E. Dudley, J.R. Wunderlich, P.F. Robbins, J.C. Yang, P. Hwu, D.J. Schwartzentruber, S.L. Topalian, R. Sherry, N.P. Restifo, A.M. Hubicki, M.R. Robinson, M. Raffeld, P. Duray, C.A. Seipp, L. Rogers-Freezer, K.E. Morton, S.A. Mavroukakis, D.E. White, S.A. Rosenberg, Cancer regression and autoimmunity in patients after clonal repopulation with antitumor lymphocytes. Science **298**, 850–854 (2002)
38. L.G. De Pillis, A.E. Radunskaya, C.L. Wiseman, A validated mathematical model of cell-mediated immune response to tumor growth. Cancer Res. **65**, 235–252 (2005)
39. A.V. Hill, The possible effects of the aggregation of the molecules of haemoglobin on its dissociation curves. J. Physiol. **40**, 4–7 (1910)
40. D.G. Mallet, L.G. De Pillis, A cellular automata model of tumor-immune system interactions. J. Theor. Biol. **239**, 334–350 (2006)
41. S.C. Ferreira Jr., M.L. Martins, M.J. Vilela, Reaction-diffusion model for the growth of avascular tumor. Phys. Rev. E **67**, 051914 (2002)
42. C.M. Cooper, R.E. Hausman, *The Cell: a molecular approach* (ASM, Washington DC, 2004)
43. C.A. Janeway, P. Travers, M. Walport, M.J. Shlomchik, *Immunobiology* (Garland Science, New York, 2012)
44. E.C. Holmes. Immunology of tumor infiltrating lymphocytes. Ann. Surg. **201**, 158–163 (1985)
45. A.G. López, J.M. Seoane, M.A.F. Sanjuán, Decay dynamics of tumors. PLoS One **11**, e0157689 (2016)
46. A.G. López, J.M. Seoane, M.A.F. Sanjuán, Destruction of solid tumors by immune cells. Commun. Nonlinear Sci. Numer. Simul. **44**, 390–403 (2017)
47. A.G. López, J.M. Seoane, M.A.F. Sanjuán, Dynamics of the cell mediated immune response. Philos. Trans. A Math. Phys. Eng. Sci. **375**, 20160291 (2017)
48. R.A. Weinberg, *The Biology of Cancer* (Garland Science, New York, 2013)
49. M. Ulberg, J. Merril, M. Jondal, Interferon induced NK augmentation in humans: an analysis of target recognition, effector cell recruitment and effector cell recycling. Scand. J. Immunol. **14**, 285–292 (1981)
50. G.E. Briggs, J.B.S. Haldane, A note on the kinematics of enzyme action. Biochem. J. **19**, 338–339 (1925)
51. G.C. Schaller, M. Meyer-Hermann, Continuum versus discrete model: a comparison for multicellular tumour spheroids. Philos. Trans. R. Soc. A **364**, 1443–1464 (2006)
52. G.P. Dunn, L.J. Old, R.D. Schreiber, The three Es of cancer immunoediting. Annu. Rev. Immunol. **22**, 329–360 (2004)
53. M.W.L. Teng, J.B. Swann, C.M. Kohebel, R.D. Schreiber, M.J. Smyth, Immune-mediated dormancy: an equilibrium with cancer. J. Leukoc. Biol. **18**, 645–653 (2008)
54. J.A. Aguirre-Ghiso, Models, mechanisms and clinical evidence for cancer dormancy. Nat. Rev. Cancer **7**, 834–846 (2007)
55. P. Paéz, M.J. Labonte, P. Bohanes, W. Zhang, L. Nebhamin, Y. Ning, T. Wakatsuki, F. Loupakis, H. Lenz, Cancer dormancy: a model of early dissemination and late cancer recurrence. Clin. Cancer Res. **18**, 645–653 (2012)
56. J.D. Farrar, K.H. Katz, J. Windsor, G. Thrush, H.S. Richard, J.W. Uhr, N.E. Street, Cancer dormancy. VII. A regulatory role for $CD8^+$ T cells and IFN-γ in establishing and maintaining the tumor-dormant state. J. Immunol. **162**, 2842–2849 (1999)
57. P.A. Gatenby, A. Basten, P. Creswick, "Sneaking through": a T-cell-dependent phenomenon. Br. J. Cancer **44**, 753–756 (1981)
58. M.J. Miller, S.H. Wei, M.D. Cahalan, I. Parker, Autonomous T cell trafficking examined in vivo with intravital two-photon microscopy. Proc. Natl. Acad. Sci. U. S. A. **100**, 2604–2609 (2003)
59. C.Y. Slaney, M.H. Kershaw, P.K. Darcy, Trafficking of T cells into tumors. Cancer Res. **74**, 7168–7174 (2014)